# Assessing the ammonium nitrate formation regime in the Paris megacity and its representation in the CHIMERE model

Hervé Petetin, Jean Sciare, Michael Bressi, Valérie Gros, Amandine Rosso, Olivier Sanchez, Roland Sarda-Estève, Jean-Eudes Petit, Matthias Beekmann

Atmos. Chem. Phys., 16, 10419–10440, 2016
www.atmos-chem-phys.net/16/10419/2016/
doi:10.5194/acp-16-10419-2016


Atmospheric Chemistry and Physics
Open Access
EGU

# Assessing the ammonium nitrate formation regime in the Paris megacity and its representation in the CHIMERE model

**Hervé Petetin[1,a], Jean Sciare[2,3], Michael Bressi[2], Valérie Gros[2], Amandine Rosso[4], Olivier Sanchez[4], Roland Sarda-Estève[2], Jean-Eudes Petit[2,b], and Matthias Beekmann[1]**

[1]LISA/IPSL, Laboratoire Interuniversitaire des Systèmes Atmosphériques, UMR CNRS 7583, Université Paris Est Créteil (UPEC) and Université Paris Diderot (UPD), France
[2]LSCE, Laboratoire des Sciences du Climat et de l'Environnement, CNRS-CEA-UVSQ, Gif-sur-Yvette, France
[3]Energy Environment Water Research Center (EEWRC), The Cyprus Institute, Nicosia, Cyprus
[4]AIRPARIF, Agence de surveillance de la qualité de l'air, Paris, France
[a]now at: Laboratoire d'Aérologie, Université Paul Sabatier and CNRS, Toulouse, France
[b]now at: Air Lorraine, Villers-les-Nancy, France

*Correspondence to:* Hervé Petetin (hervepetetin@gmail.com)

Received: 6 March 2015 – Published in Atmos. Chem. Phys. Discuss.: 3 September 2015
Revised: 2 May 2016 – Accepted: 9 May 2016 – Published: 18 August 2016

**Abstract.** Secondary inorganic compounds represent a major fraction of fine aerosol in the Paris megacity. The thermodynamics behind their formation is now relatively well constrained but, due to sparse direct measurements of their precursors (in particular $NH_3$ and $HNO_3$), uncertainties remain on their concentrations and variability as well as the formation regime of ammonium nitrate (in terms of limited species among $NH_3$ and $HNO_3$) in urban environments such as Paris. This study presents the first urban background measurements of both inorganic aerosol compounds and their gaseous precursors during several months within the city of Paris. Intense agriculture-related $NH_3$ episodes are observed in spring/summer while $HNO_3$ concentrations remain relatively low, even during summer, which leads to a $NH_3$-rich regime in Paris. The local formation of ammonium nitrate within the city appears low, despite high $NO_x$ emissions. The data set also allows evaluating the CHIMERE chemistry-transport model (CTM). Interestingly, the rather good results obtained on ammonium nitrates hide significant errors on gaseous precursors (e.g., mean bias of −75 and +195 % for $NH_3$ and $HNO_3$, respectively). This leads to a misrepresentation of the nitrate formation regime through a highly underestimated gas ratio metric (introduced by Ansari and Pandis, 1998) and a much higher sensitivity of nitrate concentrations to ammonia changes. Several uncertainty sources are investigated, pointing out the importance of better assessing both $NH_3$ agricultural emissions and OH concentrations in the future. These results remind us of the caution required when using of CTMs for emission scenario analysis, highlighting the importance of prior diagnostic and dynamic evaluations.

## 1 Introduction

Atmospheric particulate matter (PM) consists of a complex mixture of various organic and inorganic compounds known for causing serious adverse effects on human health (Chow, 2006; Pope et al., 2009), in particular close to primary sources in urban environments. Through acidic deposition, it also affects both ecosystems (Camargo and Alonso, 2006; Grantz et al., 2003) and monuments (Lombardo et al., 2013). It plays a crucial but still uncertain role in climate change through interactions with radiation and clouds formation, leading at a global scale to a radiative forcing estimated between −1.9 and −0.1 W m$^{-2}$ at a 95 % confidence interval (IPCC, 2013). Among the various chemical constituents of PM, nitrate ($NO_3^-$) contributes significantly in the form of semi-volatile ammonium nitrate to the fine (PM with aerodynamic diameter below 2.5 µm) and coarse (aerodynamic diameter between 2.5 and 10 µm) aerosol modes, with mean contributions in Europe around 6–16 and 6–20 %, respectively (Putaud et al., 2010). Several studies have reported

increasing ammonium nitrate relative contributions with increasing PM mass concentrations at urban sites, thus underlying their importance in exceedances of European PM standards (Putaud et al., 2010; Yin and Harrison, 2008). Such a pattern has been evidenced for the city of Paris by Sciare et al. (2010), Bressi et al. (2013), and Petit et al. (2015) and clearly points to the need for a better understanding of the processes controlling the formation of ammonium nitrate.

Ammonium nitrate formation primarily results from both the formation of nitric acid ($HNO_3$) and the emission of ammonia ($NH_3$) under favorable thermodynamic conditions. $NO_2$ is converted into $HNO_3$ through oxidation by the OH radical (homogeneous direct pathway) or ozone (through the formation of several intermediate compounds, including nitrate radical $NO_3\bullet$ and nitrogen pentoxide $N_2O_5$; heterogeneous indirect pathway) (Seinfeld and Pandis, 2006). The first pathway is expected to dominate during daytime, when OH concentrations are the highest (Matsumoto and Tanaka, 1996). Conversely, due to the very short lifetime of the $NO_3\bullet$ radical in the presence of solar irradiation (Vrekoussis et al., 2004), the second pathway mainly acts during nighttime, favored by decreasing temperature and increasing relative humidity (RH), or during fog events (Platt et al., 1981); Dall'Osto et al., 2009; Healy et al., 2012). Additionally, some $HNO_3$ may also be directly emitted by both anthropogenic and natural (e.g., volcanoes; Mather et al., 2004) sources. $NH_3$ is mainly emitted by agricultural activities (at 93 % in France; CITEPA, 2013), with several other minor sources including industry, traffic (e.g., Kean et al., 2009; Bishop et al., 2010; Carslaw and Rhys-Tyler, 2013; Yao et al., 2013), or sewage disposal (Sutton et al., 2000). In the presence of $NH_3$ available after the neutralization of sulfate, a thermodynamic equilibrium is reached between $HNO_3$ and $NH_3$, which potentially leads to the formation of $NH_4NO_3$ in the aqueous or solid phase, depending on temperature, RH, and sulfate concentrations (Ansari and Pandis, 1998; Mozurkewich, 1993). In marine environments, $HNO_3$ may also adsorb onto NaCl salts and react to form sodium nitrate ($NaNO_3$) in the coarse fraction (Harrison and Pio, 1983; Ottley and Harrison, 1992). The relationship between nitrate aerosols and its gaseous precursors is thus highly nonlinear (Ansari and Pandis, 1998), and the calculation of nitrate concentrations requires the use of thermodynamic models able to determine the partitioning of inorganic compounds between the gaseous and aerosol (aqueous or solid) phases depending on the temperature and RH conditions (see Fountoukis and Nenes, 2007 for a review).

Considering the high contribution of nitrate to fine particulate pollution, both the identification of the limited species (among $NH_3$ and $HNO_3$) in the formation of $NH_4NO_3$ and the quantification of the PM response to a given emission reduction of either precursor are crucial information for air quality management authorities in charge of designing efficient PM control strategies. Various approaches have been proposed in the literature to investigate these points. Chemistry-transport model (CTM) simulations and emission reduction scenarios remain the easiest way to provide a first guess of the limited species and PM response to emission changes. Over Europe, several studies with different CTMs have simulated a $HNO_3$-limited regime (Sartelet et al., 2007; Kim et al., 2011, with the POLYPHEMUS model; Hamaoui-Laguel et al., 2014, with the CHIMERE model; Pay et al., 2012, with the CALIOPE-EU modeling system). However, such an approach relies on the good performance of CTMs that still suffer from various uncertainties, in particular in their input data (e.g., emission inventories). With respect to these perspectives, comparisons with field observations are highly valuable for evaluating model outputs. When measurements of total nitrate ($TNO_3 = HNO_{3(g)} + NO_3^-$), total ammonia ($TNH_3 = NH_{3(g)} + NH_4^+$), and total sulfate ($TS = H_2SO_{4(g)} + HSO_4^- + SO_4^{2-}$) are available, it is possible to diagnose which precursor is limiting nitrate formation. A first approach relies on the use of the gas ratio (GR) defined as the ratio of free ammonia after sulfate neutralization ($FNH_x(\mu mol\,m^{-3}) = NH_3 + NH_4^+ - 2\times SO_4^{2-}$) to total nitrate ($TNO_3(\mu mol\,m^{-3}) = HNO_3 + NO_3^-$) (Ansari and Pandis, 1998). GR values above unity indicate a regime mainly limited by $HNO_3$ (e.g., $NH_3$-rich regime) in which there is enough $NH_3$ to neutralize both sulfate and nitrate. Conversely, GRs between 0 and 1 indicate that there is enough $NH_3$ to neutralize sulfate but not nitrate, while negative GRs correspond to a $NH_3$-poor regime in which $NH_3$ amounts are insufficient to even neutralize sulfate. Based on the European Monitoring and Evaluation Program (EMEP) regional background observations, Pay et al. (2012) obtained GRs above unity (i.e., a $HNO_3$-limited regime) over continental Europe, in reasonable agreement with the CALIOPE model. Conversely, a $NH_3$-limited regime was found over ocean and closer to coasts in some countries (e.g., Spain, England, countries around Baltic Sea) due to ship emissions of $SO_2$ and $NO_x$ and low $NH_3$ over marine regions. However, the determination of the limited compound based on GR is valid only under the assumption of a complete transfer (of the limited species) in the aerosol phase (i.e., at low temperature and high RH). Under ambient conditions favoring a partitioning between both phases, both $NH_3$ and $HNO_3$ exist in the gas phase and the nitrate formation may be sensitive to changes in one or the other precursor. A more realistic assessment of the nitrate formation regime can be obtained by performing sensitivity tests on thermodynamic models fed by field measurements (concentrations, temperature, and RH). Such an approach allows quantifying the PM response to total reservoir ($TNH_3$, $TNO_3$, or TS) concentration reductions (Ansari and Pandis, 1998; Takahama et al., 2004 with the GFEMN model; Blanchard and Hidy, 2003, with the SCAPE2 model). These studies rely on the hypothesis that the concentration reduction of one specific compound does not affect the others, which is not true due to lifetime differences between gas and aerosol phases induced by contrasted

deposition rates; for instance, a reduction of sulfate increases the amount of $FNH_x$ available for the formation of nitrate that deposit less than $HNO_3$ (Davidson and Wu, 1990), which finally increases the $TNO_3$ reservoir. These difficulties may be overcome through the combined use of observations and deposition parameterizations in observation-based box models (Vayenas et al., 2005). As these models cannot integrate the whole complexity at stake in the atmosphere, CTMs are still needed to assess the nitrate formation regime and the PM response to precursors changes, but they require in turn validation by experimental data.

This paper aims at investigating the variability and sources of both $HNO_3$ and $NH_3$, as well as the associated $NH_4NO_3$ formation regime in the Paris megacity and the ability of the CHIMERE regional CTM to reproduce it. To this end, an important experimental effort, in the framework of the PARTICULES and FRANCIPOL projects, has recently made available a large database of fine aerosol chemical compounds (e.g., nitrate, ammonium, sulfate) and inorganic gaseous precursors (e.g., $HNO_3$, $NH_3$) in the region of Paris. To our knowledge, this is the first time that simultaneous measurements of inorganic compounds in both gaseous and aerosol phases, covering most seasons, are performed in France. Experimental aspects are described in Sect. 2. The CHIMERE model and its setup is then introduced in Sect. 3. Results are shown and discussed in Sect. 4, and overall conclusions are given in Sect. 5.

## 2 Experimental

### 2.1 Fine aerosols measurements

As part of the AIRPARIF-LSCE "PARTICULES" project (Airparif, 2011, 2012), fine aerosol particles ($PM_{2.5}$) were collected every day for 24 h (from 00:00 to 23:59 LT) during 1 year (from 11 September 2009 to 10 September 2010) using two collocated Leckel low volume samplers (SEQ47/50) running at $2.3\,m^3\,h^{-1}$. One Leckel sampler was equipped with quartz filters (QMA, Whatman, 47 mm diameter) for carbon analyses, the second with Teflon filters (PTFE, Pall, 47 mm diameter, 2.0 µm porosity) for gravimetric and ion measurements (including $NH_4^+$, $NO_3^-$, and $SO_4^{2-}$). Six sampling sites were implemented, covering the region of Paris. Only the results for the background station located in the city center of Paris (fourth district; 48°50′56″ N, 02°21′55″ E; 20 m a.g.l.) will be presented here. More information on the experimental setup and quality control of the data sets is available in Bressi et al. (2013). Note that filter measurements are subject to artifacts, through the evaporation and/or the adsorption of semi-volatile compounds (Pang et al., 2002), and thus mostly affect ammonium nitrate and organic matter concentrations. Daily chemical mass closure studies and comparisons with online artifact-free measurements were performed for that purpose and showed that filter sampling was quite systematically missing about 20 % of $PM_{2.5}$ (15 % of fine nitrate; Bressi et al., 2013).

### 2.2 Gaseous precursors measurements

As part of the PRIMEQUAL (Programme de Recherche Interorganisme pour une MEilleure QUalité de l'Air à l'échelle Locale) "FRANCIPOL" project, gaseous precursors ($NH_3$, $HNO_3$, $SO_2$) were monitored in near real time on the roof platform (14 m a.g.l.) at the Laboratoire d'Hygiène de la Ville de Paris (LHVP) in the heart of Paris (13th district). Gas-phase $NH_3$ measurements were obtained for a 10-month period (May 2010–February 2011) every 5 min using an AiRRmonia monitor (Mechatronics Instruments BV, The Netherland). The March/April periods (2010 and 2011) were missing due to technical problems with the instrument. Based on conductivity detection of $NH_4^+$, gaseous $NH_3$ were sampled at $1\,L\,min^{-1}$ using a 1 m long Teflon (0.5 in. diameter) sampling line. It was then collected through a sampling block equipped with an $NH_3$-permeable membrane; a demineralized water counter-flow allows $NH_3$ to solubilize in $NH_4^+$. A second purification step was applied by adding 0.5 mM sodium hydroxide, leading to the detection of $NH_4^+$ in the detector block. The instrument was calibrated regularly (twice per months) using 0 and 500 ppb $NH_4^+$ aqueous solution (NIST standards). Two sets of sampling syringes ensure a constant flow throughout the instrument but also create a temporal shift, ranging from 10 to 40 min in different studies (Erisman et al., 2001; Cowen et al., 2004; Zechmeister-Boltenstern, 2010; von Brobrutzki et al., 2010). We have taken here a constant value of 30 min for this delay in time response. Detection limit and precision of the instrument are typically $0.1\,\mu g\,m^{-3}$ and 3 to 10 %, respectively (Erisman et al., 2001; Norman et al., 2009). More than 62 000 valid data points of $NH_3$ – covering 217 days – were obtained with the AiRRmonia instrument and used for this study.

$HNO_3$ and $SO_2$ were analyzed continuously for an 11-month period (March 2010–January 2011) using a wet annular denuder (WAD) similar to the one reported in details by Trebs et al. (2004) and coupled with ion chromatography (IC). Briefly, whole air was sampled at $\sim 10\,L\,min^{-1}$ in the WAD. This air flow rate – slightly below the $17\,L\,min^{-1}$ usually set – was taken to ensure a laminar flow and minimize particle losses onto the walls of the WAD and thus minimize possible artifacts in our IC (anion) measurements that could raise from inorganic salts present in the particulate phase. Following the recommendations by Neuman et al. (1999), our sampling line was made of plastic (PE, 0.5 in. diameter, John Guest, USA) and reduced to 1 m in order to keep a residence time of sampled air below 1 s preventing formation/losses of $NH_4NO_3$ (Dlugi, 1993). 18.2 MΩ water was used to rinse the WAD at a flow rate of $\sim 0.40\,mL\,min^{-1}$ and feed the IC with the solubilized acid gases. The IC (ICS2000, Dionex) configuration setup is similar to the one reported by (Sciare et al., 2011). Time resolution (chromatogram)

was typically 15 min for the major gaseous acidic species (HCOOH, $CH_3COOH$, HCl, HONO, $HNO_3$, $SO_2$). Oxidation of $SO_2$ into $SO_4^{2-}$ in the liquid flow downstream of the WAD was performed by solubilization of ambient oxidants such as $H_2O_2$. Based on these settings, detection limit for acidic gases was typically below $0.1\,\mu g\,m^{-3}$. Uncertainties in ambient concentrations of acidic gases depend on air and liquid flow rates (controlled on a weekly basis) as well as the IC calibration (performed every 2 months). Overall standard deviations ($1\sigma$) of 6, 15, and 10 % were calculated for these three parameters (air flow rate, liquid flow rate, IC calibration), respectively, leading to a total uncertainty of about 20 % for the WAD–IC measurements.

This WAD technique has been successfully intercompared with offline techniques in Trebs et al. (2008). Further comparison of the WAD–IC technique was performed during our study with a commercially available $SO_2$ analyzer (AFM22, Environnement S.A.) for a period of 3 months. Despite the poor detection limit ($1\,ppb = 2.43\,\mu g\,m^{-3}$) of the commercially available instrument and the low ambient concentrations recorded at our station with $SO_2$ monthly means ranging from 0.76 to $3.03\,\mu g\,m^{-3}$ measured with our WAD–IC instrument, quite consistent results were obtained from this intercomparison (slope of 0.73 and $r^2 = 0.56$ for $n = 1671$ hourly averaged data points). More than 24 000 valid data points of $SO_2$ and $HNO_3$ – covering 253 days – were obtained with the WAD–IC instrument and used for this study.

### 2.3 Meteorological parameters measurement

Beside chemical compounds, traditional meteorological parameters – temperature, wind speed and direction, RH – are also measured at the MONTSOURIS station (2.337° E, 48.822° N) in Paris, close to the LHVP site (∼ 2 km). In addition, boundary layer height (BLH) estimations are retrieved from an aerosol lidar at the SIRTA (Site Instrumental de Recherche par Télédetection Atmosphérique) site (48.712° N, 2.208° E) (Haeffelin et al., 2012).

This paper will focus on measurements performed from 1 April to 31 December 2010. Note that all the measurements described in previous sections come from different campaigns and measurement periods that do not entirely overlap. Measurements of secondary inorganic aerosols ($NH_4^+$, $NO_3^-$, $SO_4^{2-}$) are available daily between 1 April and 10 September 2010. $NH_3$ ($HNO_3$) observations are available hourly from 20 May (1 April) to 31 December 2010.

### 2.4 Representativeness and data set combination

The purpose of this study is to investigate the relation of $NH_4NO_3$ with its gaseous precursors, which ideally requires co-located measurements of all compounds in both phases. This was not the initial purpose of PARTICULES and FRANCIPOL projects, and thus no such co-located observations are available in Paris. However, we argue here that the two data sets (inorganic aerosols measured in the 4th district of Paris and gaseous precursors measured in the 13th district) can be reasonably considered as co-located and representative of the urban background of at least the southern half of the Paris city.

Several elements support this hypothesis. First, both sites are only ∼ 3 km away from each other. Second, both sites are located on the rooftop of rather high buildings (20 and 14 m a.g.l.), thus quite far from direct influence of local pollution sources (e.g., traffic) and at a height where the venting of pollution is favored by the absence of obstacles and likely stronger winds (compared to the street level). The height of the LHVP roof site is slightly lower compared to the other site, but the building is located in a public garden, which further limits the possibility of local contamination by surrounding pollution sources. Third, based on the $PM_{2.5}$ chemical speciation measurements performed both inside Paris and at several rural sites all around the Paris region during a whole year, the PARTICULES project has shown that secondary inorganic aerosols in the Paris urban background are mostly imported from outside the city (Petetin et al., 2014). At the annual scale, the contribution of imports was estimated to be 78 % for nitrate, 90 % for ammonium, and 98 % for sulfate (see Table 6 in Petetin et al., 2014). This is mostly explained by (i) the presence of strong pollution reservoirs in Europe (e.g., Benelux, eastern Europe) from where large plumes can be advected toward Paris under certain meteorological conditions; (ii) the time necessary for the formation of inorganic aerosols (including the oxidation of $NO_x$ and $SO_2$) is too low to allow a strong local production that thus preferentially occurs downwind in the Paris plume, as observed during the MEGAPOLI campaign (Freney et al., 2014); and (iii) the limited occurrence of stagnant conditions in Paris (that would allow enough time for gaseous precursors to produce inorganic aerosols). The high contribution of imported pollution is confirmed by the comparison of daily inorganic aerosol concentrations between the fourth district site and a traffic site located along the Paris ring 8 km westward, that shows a very good correlation for all inorganic aerosols during the whole year (ammonium: $y = 0.95x + 0.02$, $R = 0.97$, $N = 325$; nitrate: $y = 0.99x - 0.09$, $R = 0.98$, $N = 325$; sulfate: $y = 1.04x + 0.01$, $R = 0.98$, $N = 325$). Thus, concerning secondary inorganic aerosols, the urban background can be considered as rather homogeneous at the scale of the whole Paris agglomeration. Additionally, observations in the fourth district of Paris can be reasonably combined to gaseous precursors observations at the other site.

In terms of spatial representativeness for $HNO_3$ and $NH_3$, no other measurements are available to quantitatively assess the homogeneity of their urban background. In particular, some $NO_x$ emitted within the center of the city may be already converted into $HNO_3$ at the borders of the Paris agglomeration, leading to higher concentrations compared to the center of Paris. Thus, one cannot a priori consider these

measurements representative of the urban background at the scale of the whole Paris agglomeration. However, as we already discussed, considering the morphology and the geographical location of the LHVP site, one can reasonably consider that it is representative of the urban background of at least the southern half of Paris city.

## 3 Model setup and input data

### 3.1 CHIMERE model description

Simulations are performed using the CHIMERE CTM (Schmidt and Derognat, 2001; Bessagnet et al., 2009; Menut et al., 2013) (www.lmd.polytechnique.fr/chimere), which is designed to provide short-term predictions of ozone and aerosols, as well as to help emissions mitigation assessment through emission reduction scenarios. It is used both in research activities and operational air quality monitoring and forecasting at the local, national, and European scale (ESMERALDA over the northern part of France; PREVAIR service, www.prevair.org; GMES-MACC program).

The CHIMERE model includes the MELCHIOR2 (ModEle CHImique de l'Ozone à l'échelle Régionale) chemical mechanism (around 40 species and 120 reactions) for the gas-phase chemistry, some aqueous-phase (e.g., aqueous pathways for sulfate production) and heterogeneous (e.g., $HNO_3$ formation on existing particles and fog droplets, including the conversion of $N_2O_5$) reactions, and size-dependent aerosol compounds (nine bins ranging from 40 nm to 20 µm diameters), including secondary organic and inorganic aerosols. Dry and wet deposition of gaseous and aerosol species is parameterized from three types of sequential resistances following the resistance analogy (Wesely, 1989). An aerodynamical resistance is estimated based on turbulent parameters (e.g., Monin–Obukhov length, friction velocity, dynamical roughness length). A quasi-laminary boundary layer resistance is calculated based on the molecular diffusivity of water and gaseous species and Prandtl number. The surface resistance of vegetation and soils is estimated from several parallel resistances related to plant surfaces via opening of stomata and related to non-stomatal deposition at plant and soil surfaces (Erisman et al., 1994). The scavenging of gases and particles, both in clouds and rain droplets, is included in CHIMERE. The scavenging of $HNO_3$ and $NH_3$ by cloud droplets (in rain droplets) is assumed reversible (irreversible). In clouds, particles can be scavenged by coagulation with cloud droplets or by precipitation or can act as cloud condensation nuclei to form new droplets. Particles can also be scavenged by raining drops below the clouds. More details can be found in Menut et al. (2013). The model also includes a parameterization for the coagulation, absorption, and nucleation aerosol processes.

Inorganic species are treated using the ISORROPIA thermodynamic equilibrium model (Nenes et al., 1998), considering only the $NH_3$–$HNO_3$–$H_2SO_4$–$H_2O$ system. ISORROPIA follows a bulk aerosol approach (without any consideration of the aerosol size distribution) and assumes an instantaneous equilibrium in the gas–aerosol system, as well as no influence of other compounds (in particular, the soluble organic matter). Given the temperature, RH, $TNO_3$, $TNH_3$, and TS (assuming that $TS = SO_4^{2-}$ due to low concentrations of $H_2SO_4$ and $HSO_3$ in the aerosol phase), the partitioning coefficient between both aerosol and gas phases at equilibrium is computed and used to drive the system toward the corresponding direction (thus countering the hypothesis of an instantaneous equilibrium assumed in ISORROPIA). For calculation efficiency, the model is not used online but through a tabulated version designed to cover a large range of meteorological conditions with temperature ranging from 260 to 312 K (increment +2.5 K), RH from 0.3 to 0.99 (increment +0.05), and TS, $TNO_3$, and $TNH_3$ concentrations from $10^{-2}$ to 65 µg $m^{-3}$ (increment ×1.5) (Menut et al., 2013).

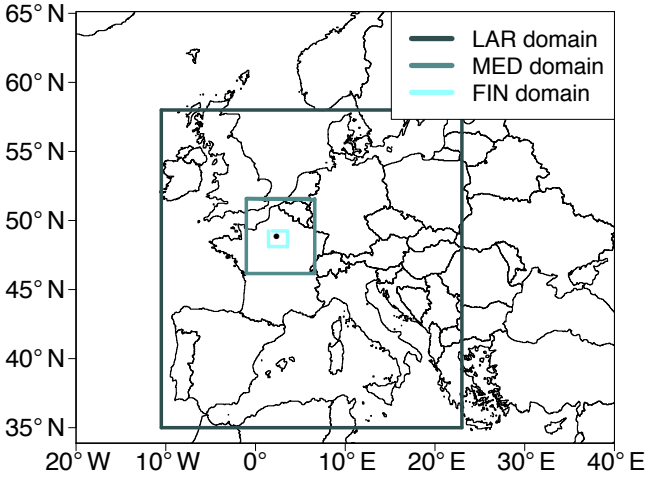


**Figure 1.** Nested domains (the black points in the finest domain indicates Paris). Resolutions are 0.5 × 0.5° (LAR domain), 9 × 9 km (MED), and 3 × 3 (FIN).

### 3.2 Model configuration

As shown in Fig. 1, three nested domains are used for all simulations – a large (LAR), a medium (MED), and a fine (FIN) domain – with horizontal resolutions increasing from 0.5 × 0.5° (roughly 50 × 50 km), 9 × 9 km and 3 × 3 km, respectively. A discretization of eight levels, from 40 m to 5 km a.g.l., is applied on the vertical dimension.

Meteorological inputs are provided by PSU/NCAR MM5 simulations (Dudhia, 1993) using boundary conditions and large-scale data coming from the Final Analyses (FNL) data from the National Centers for Environmental Prediction (NCEP) (http://rda.ucar.edu/datasets/ds083.2).

Gaseous and aerosol emissions in all domains come from the so-called TNO-MP (MP for MegaPoli) inventory. De-

veloped in the framework of the European MEGAPOLI (Megacity: emission, urban, regional, and global atmospheric pollution and climate effect, and integrated tools for assessment and mitigation; www.megapoli.info) project (Baklanov et al., 2010), this highly resolved ($0.125 \times 0.0625°$, i.e., roughly $7 \times 7$ km) European inventory is based on the TNO inventory (Denier van der Gon et al., 2010; Pouliot et al., 2012; Kuenen et al., 2011, 2014), but it incorporates bottom-up emission data (compiled by local authorities such as Airparif for Paris; Airparif, 2010) over the four European megacities (Paris, London, Rhine-Ruhr, and Po valley) (see Denier van der Gon et al., 2011, for more details). The region of Paris roughly corresponds to the FIN domain. In order to reach the CHIMERE resolution, emissions are downscaled based on the $1 \times 1$ km resolved GLCF (Global Land Cover Facility) land use database (Hansen et al., 2000) and apportioned according to the type of land use (Menut et al., 2013).

Boundary and initial conditions come from the LMDZ-INCA2 (Folberth et al., 2006) global model for gaseous species and the LMDZ-AERO (Folberth et al., 2006; Hauglustaine, 2004) for particulate species. Biogenic emissions are computed from the MEGAN model using parameterizations from Guenther et al. (2006).

This reference simulation will be referred to as the MOD case. A second simulation is performed without any local anthropogenic emissions from the region of Paris (in the three nested domains), in order to assess the influence of imported pollution over the city of Paris. It will be referred to as the MOD-noIDF case (IDF for Île-de-France, the name of the region of Paris). In addition, as $NH_3$ is strongly impacted by dry deposition in which high uncertainties persist (e.g., Flechard et al., 2011), a third simulation (so-called MOD-nodep) is performed without any $NH_3$ dry deposition over the entire domain in order to investigate its influence on concentrations within Paris.

## 4 Results

The following subsections present results on sulfate and $SO_2$ (Sect. 4.1), $NH_3$ (Sect. 4.2), and $HNO_3$ (Sect. 4.3). For all compounds, the temporal variability given by measurements is assessed at different scales (monthly, daily, and diurnal), as well as the model's ability to reproduce the observed concentrations. For the analysis of air mass origins, back trajectories have been calculated during the whole period with the FLEXTRA model (Stohl et al., 2001) using the same MM5 meteorology as in the CHIMERE simulations. The FLEXTRA simulations are performed by releasing, every 6 h, 10 particles around the center of Paris, starting at 500 m altitude, which leads to a daily set of 40 back trajectories. Several uncertainty sources in the model (or input data) are also discussed. The nitrate formation regime in terms of limiting species among $NH_3$ and $HNO_3$, the nitrate simulation in CHIMERE as well as the nitrate response to changes in precursors concentrations are then characterized in Sect. 4.4.

Statistical metrics used in the evaluation of the CHIMERE results compared to observations are defined as follows.

$$\text{Mean bias (MB)} = \frac{1}{n}\sum_{i=1}^{n}(m_i - o_i) \quad (1)$$

$$\text{Normalized mean bias (NMB)} = \frac{\frac{1}{n}\sum_{i=1}^{n}(m_i - o_i)}{\bar{o}} \quad (2)$$

$$\text{Root mean square error (RMSE)} = \sqrt{\frac{1}{n}\sum_{i=1}^{n}(m_i - o_i)^2} \quad (3)$$

Normalized root mean square error

$$\text{(NRMSE)} = \frac{\sqrt{\frac{1}{n}\sum_{i=1}^{n}(m_i - o_i)^2}}{\bar{o}} \quad (4)$$

Correlation coefficient

$$R = \frac{\sum_{i=1}^{n}(m_i - \bar{m})(o_i - \bar{o})}{\sqrt{\sum_{i=1}^{n}(m_i - \bar{m})^2 \sum_{i=1}^{n}(o_i - \bar{o})^2}}, \quad (5)$$

where $m_i$ and $o_i$ are the modeled and observed concentrations at time $i$, respectively, and $\bar{m}$ and $\bar{o}$ their average over a given period.

### 4.1 Sulfate and $SO_2$

Sulfate daily concentrations in Paris are given in Fig. 2. The variability of sulfate (as of nitrate) during the PARTICULES campaign has been discussed in details in Bressi et al. (2013). Fine ($PM_{2.5}$) sulfate concentrations range between 0.4 and 5.0 $\mu g\,m^{-3}$ (one high value at 8.7 $\mu g\,m^{-3}$), with an average of 2.0 $\mu g\,m^{-3}$ over the studied period (1 April–10 September). The episodes with highest concentrations are associated with air masses originating from the north/northeast, also noted by Bressi et al. (2013), Petetin et al. (2014) and Petit et al. (2015). Despite a faster $SO_2$-to-sulfate conversion due to higher OH levels in summer, lower concentrations are measured during that season due to a combination of lower $SO_2$ emissions and a dominant marine regime, with relatively clean air masses originating from west and southwest and slightly more polluted ones from northwest.

During the period of available data (152 days in spring and summer), $NH_3$ levels are high enough to fully neutralize both sulfate and nitrate, as indicated by the linear regression of $NH_4^+$ vs. $NO_3^- + 2SO_4^{2-}$ daily concentrations in the fine mode that gives a slope of 1.01, a $y$ intercept of $-0.20$ ppb, and a correlation coefficient ($r^2$) of 0.97 ($n = 150$; see Fig. S1 in the Supplement). Note that plotting all major cations ($Na^+ + NH_4^+ + K^+ + 2Ca^{2+} + 2Mg^{2+}$) against

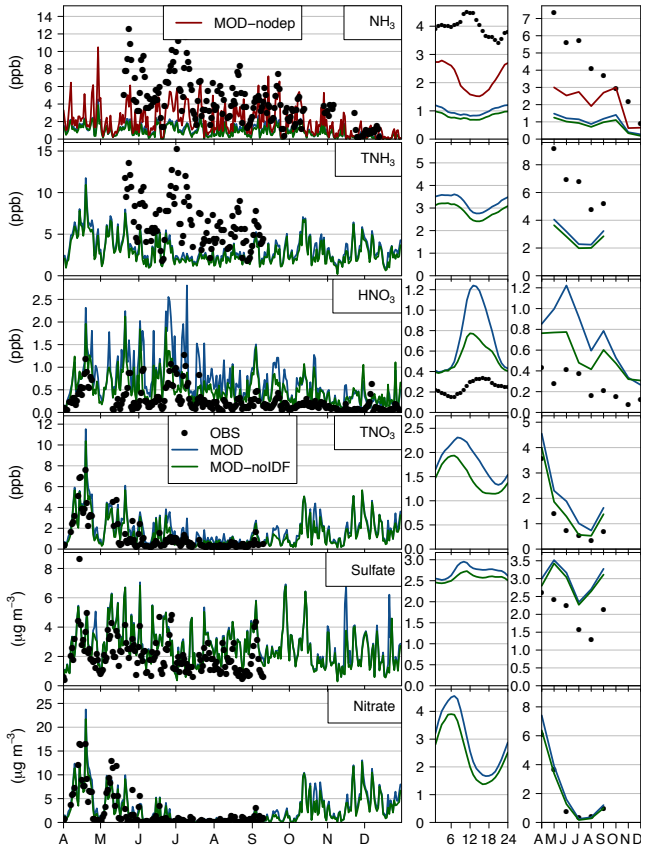


**Figure 2.** Observed and modeled daily averaged concentrations (left panel), diurnal profiles (middle panel), and monthly concentrations (right panel). MOD-nodep results are only shown for $NH_3$. Note: CHIMERE monthly concentrations are computed including only days with available observational data. For particulate matter observations, only daily values are available.

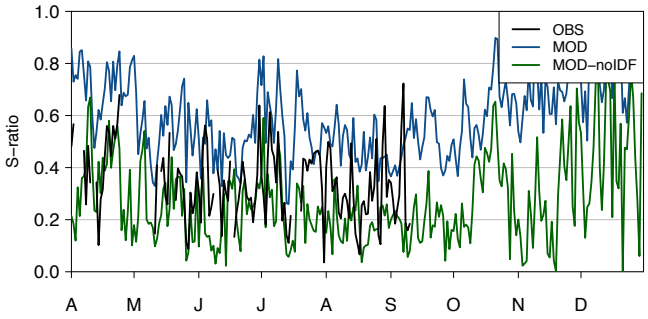


**Figure 3.** Observed and modeled (with – MOD case – and without – MOD-noIDF case – emissions over the Paris region) daily S ratio in Paris.

all major anions ($NO_3^- + 2SO_4^{2-} + Cl^-$) leads to a slope of 1.03, a $y$ intercept of +0.13 ppb, and a correlation of 0.97, demonstrating the neutrality of our fine aerosol.

Statistical results of modeled vs. measured concentrations are reported in Table 1. The model partially reproduces the day-to-day variability of sulfate concentrations ($r = 0.59$), but overestimates concentrations, with a NMB of +48 % and a NRMSE of 74 %. This does not appear to be related to a too high $SO_2$-to-sulfate conversion since $SO_2$ concentrations are significantly overestimated in Paris, by about a factor of 3 (Table 1). This is also suggested by the simulated S ratio. This indicator – defined as the ratio of $SO_2$ over $SO_2+SO_4^{2-}$, all concentrations being expressed in µg m$^{-3}$ (Hass et al., 2003; Pay et al., 2012) – allows us to assess how strongly oxidized is a plume containing sulfur. High S ratios are found in air masses containing freshly emitted $SO_2$, while low S ratios are associated with older air masses in which more $SO_2$ has already been converted into sulfate. The observed and simulated S ratios are shown in Fig. 3 (the $SO_2+SO_4^{2-}$ time series is shown in Fig. S4 in the Supplement). In the MOD simulation, CHIMERE clearly overestimates the S ratio (average value of 0.54 vs. 0.34 for the observations); i.e., the simulated air masses contain too much freshly emitted $SO_2$ compared to reality. Such a high bias on $SO_2$ concentrations is not expected but does not appear representative of the CHIMERE performance at a larger scale. Considering the $SO_2$ observations available at nine urban background sites (AIRPARIF operational network) in the region of Paris, NMB are lower, ranging from +24 to +160 %. As a large part of $SO_2$ is emitted by point sources, the dilution effect in a $3 \times 3$ km cell remains a well-known uncertainty source at stations potentially impacted by plumes coming from nearby industrial facilities. However, in our case, large $SO_2$ industrial point sources are relatively far from our background urban station, and emissions from non-point sources (i.e., on-road transport and residential sectors) remain important in the center of Paris, which suggests potential errors on the Paris agglomeration emissions (overestimation of total emissions, wrong vertical allocation) and/or the BLH. Indeed, the average $SO_2$ diurnal profile shows maximum discrepancies (up to a factor of 4.8) during the transition from a convective to a nocturnal boundary layer. This transition occurs too early in the model (see Fig. S3 in the Supplement), which likely explains a noticeable part of the bias for $SO_2$. Conversely, the sulfate overestimation may be due to errors during the transport of air masses from northeastern Europe.

## 4.2 Ammonia

### 4.2.1 Temporal variability

Daily averaged concentrations and diurnal profiles of $NH_3$ are given in Fig. 2. The model results will be discussed in the next section. According to the review of Reche et al. (2012), $NH_3$ concentrations in worldwide urban environments range between 0.4 and 63.6 ppb, thus spanning over 2 orders of magnitude. On a logarithmic scale, the average concentration of 4.0 ppb measured in Paris over the whole period is roughly in the middle range of this range. It is also consistent

**Table 1.** Statistical results at our urban background sites over the whole period (all statistical metrics are defined at the beginning of Sect. 4; MO is the observed concentration mean, *N* the data coverage).

| Species | Case | MO | MB | NMB (%) | RMSE | NRMSE (%) | *R* | *N* (%) |
|---|---|---|---|---|---|---|---|---|
| $NH_3$* (ppb) | MOD | 4.0 | −3.0 | −75 | 3.9 | 99 | 0.42 | 64 |
| | MOD-noIDF | | −3.1 | −79 | 4.1 | 103 | 0.39 | 64 |
| | MOD-nodep | | −1.8 | −46 | 3.2 | 82 | 0.45 | 64 |
| $HNO_3$* (ppb) | MOD | 0.3 | +0.5 | +195 | 0.8 | 320 | 0.56 | 81 |
| | MOD-noIDF | | +0.3 | +120 | 0.6 | 219 | 0.36 | 81 |
| $SO_2$* (ppb) | MOD | 0.5 | +1.0 | +194 | 1.6 | 303 | 0.38 | 83 |
| | MOD-noIDF | | −0.1 | −20 | 0.9 | 170 | 0.25 | 83 |
| Ammonium ($\mu g\,m^{-3}$) | MOD | 1.2 | +0.4 | +35 | 0.9 | 70 | 0.84 | 54 |
| | MOD-noIDF | | +0.3 | +23 | 0.8 | 64 | 0.84 | 54 |
| Nitrate ($\mu g\,m^{-3}$) | MOD | 2.1 | +0.4 | +19 | 2.2 | 109 | 0.81 | 54 |
| | MOD-noIDF | | +0.0 | +1 | 2.1 | 101 | 0.81 | 54 |
| Sulfate ($\mu g\,m^{-3}$) | MOD | 2.0 | +1.0 | +48 | 1.5 | 74 | 0.59 | 54 |
| | MOD-noIDF | | +0.9 | +42 | 1.4 | 69 | 0.61 | 54 |
| F-NHx (ppb) | MOD | 5.5 | −4.1 | −75 | 4.7 | 87 | 0.51 | 37 |
| | MOD-noIDF | | −4.4 | −80 | 5.0 | 92 | 0.48 | 37 |
| S ratio | MOD | 0.3 | +0.2 | +60 | 0.3 | 73 | 0.46 | 48 |
| | MOD-noIDF | | −0.1 | −29 | 0.2 | 55 | 0.33 | 48 |
| GR ($ppb\,ppb^{-1}$) | MOD | 12.6 | −11.4 | −90 | 14.2 | 112 | 0.37 | 36 |
| | MOD-noIDF | | −11.2 | −88 | 14.0 | 111 | 0.33 | 36 |
| $TNH_3$ (ppb) | MOD | 6.4 | −3.6 | −56 | 4.4 | 70 | 0.43 | 37 |
| | MOD-noIDF | | −3.9 | −61 | 4.7 | 74 | 0.40 | 37 |
| $TNO_3$ (ppb) | MOD | 1.1 | +0.8 | +71 | 1.3 | 123 | 0.78 | 47 |
| | MOD-noIDF | | +0.3 | +31 | 1.1 | 97 | 0.79 | 47 |

* Statistics based on hourly data (otherwise, daily data are used).

with the values obtained in other European cities: 4.4 ppb in Aveiro (Portugal, August–May), 5.2 ppb in Roma (Italy, May–March), 5.5 ppb in Münster (Germany, May–June), 3.2 in Thessaloniki (Greece, year), 3.9–10.6 in Barcelona (Spain, July and January), and 3.1 ppb in Schiedam (the Netherlands, winter) (Reche et al., 2012, and references therein). $NH_3$ concentrations in Paris show a large variability (illustrated by a standard deviation of 2.8 ppb) with several elevated $NH_3$ episodes in late spring and early summer (hourly concentrations reaching up to 18.5 ppb in June), moderate concentrations in late summer, and lower ones in autumn and winter. On average, the observed $NH_3$ diurnal profile (Fig. 2) is rather flat, with slightly increasing concentrations in the morning leading to a maximum at 10:00–13:00 UTC. Concentrations decrease in the afternoon up to a minimum at 20:00 UTC. The diurnal variability of $NH_3$ depends on many factors, including the strength of local emission sources, the dry deposition, the evolution of the BLH, the formation of $NH_4NO_3$ during the night promoted by larger RH, and its thermodynamically driven evaporation during the daytime (Wichink Kruit et al., 2007). The daytime increase may be partly due to this volatilization of $NH_4NO_3$.

**Influence of temperature**

Figure 4 shows the $NH_3$ concentrations in function of the temperature. Both appear clearly linked in Paris, the highest episodes occurring concomitantly with the warmest conditions (see the meteorology evaluation in the Supplement, Sect. S2). The lower sensitivity to temperature in the model will be discussed later. Such a relation between $NH_3$ and the temperature has already been observed in other cities (e.g., Perrino et al., 2002; Gong et al., 2011; Reche et al., 2012). Temperature and RH strongly influence the equilibrium constant governing the partitioning of inorganic compounds between the gas and aerosol phases, with higher $NH_3$ concentrations expected when the temperature is high and the RH is low due to the volatilization of $NH_4NO_3$. In addition, several $NH_3$ emission sources may be enhanced by high temperature, including the agricultural (e.g., volatilization of fertilizer) or biological sources.

The link between $NH_3$ and temperature can be illustrated by the early July episode when, in parallel with the temperature increase between 30 June and 2 July, the $NH_3$ baseline progressively increases in Paris, up to 18.5 ppb at the hourly scale (the maximum over the whole FRANCIPOL period). A part of the $NH_3$ increase is likely due to evaporation of $NH_4NO_3$, but in early July a similar episode is observed for $TNH_3$, which means that an additional $NH_3$ source is present.

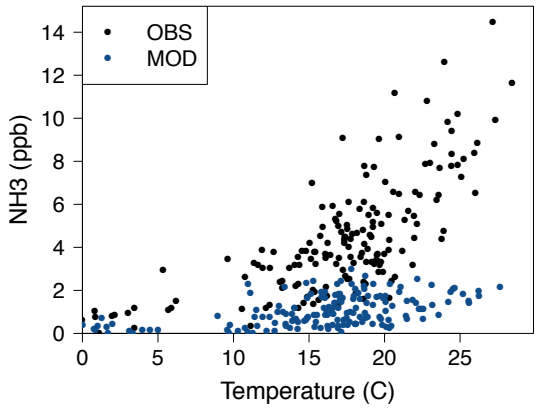


**Figure 4.** Daily observed (in black) and modeled (in blue) $NH_3$ concentrations vs. temperature in Paris (for the model, only days with available observations are plotted).

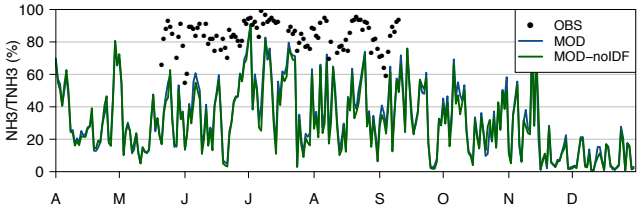


**Figure 5.** Daily $NH_3$ / $TNH_3$ ratios in observations (points) and simulations (solid lines).

The $NH_3$/ $TNH_3$ ratios are shown in Fig. 5. The experimentally determined $TNH_3$ is clearly dominated by $NH_3$ that has a contribution around 55–99 % (83 % on average). Negative artifacts on the $NH_4^+$ filter measurements cannot be excluded (in particular during summertime), but increasing $NH_4^+$ concentrations by 50 % has a very limited impact ($NH_3$ contributions ranging in that case around 45–99 %, 78 % on average).

### Influence of traffic $NH_3$

Several studies have previously addressed the question of the $NH_3$ emitted by the traffic in urban areas, although with more or less contrasted and definitive conclusions depending on the city (e.g., Perrino et al., 2002; Gong et al., 2011). The difficulty notably arises from the short lifetime of $NH_3$ that can quickly deposit on the ground, be diluted or converted into $NH_4^+$. In Paris, the diurnal profile does not show any peak at morning and evening rush hours, even during periods of lower agricultural emissions (e.g., August and September; too few data in winter). This suggests that traffic emissions are probably a relatively minor source during our study. This is supported by the low correlation of black carbon (BC) (mainly emitted by the traffic) and $NH_3$ concentrations measured at the LHVP site ($r = 0.20$ over the whole period). However, it is worth noting that during the end of June episode, the hourly time series shows some morning

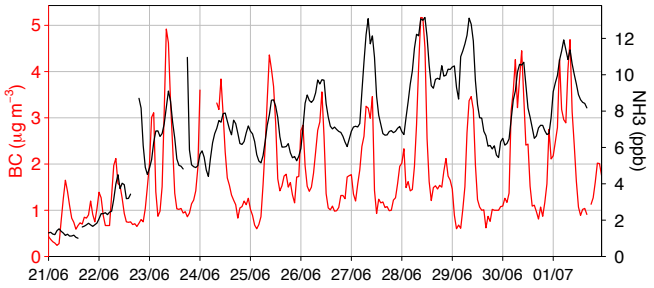


**Figure 6.** Observed BC (in red) and $NH_3$ (in black) hourly concentrations at LHVP during the end of June.

peaks (above an increasing background line likely due to the advection of agricultural $NH_3$) that may be associated to traffic $NH_3$ emissions, as illustrated by the increased correlation with BC ($r = 0.60$ between the 21 June and 3 July) (Fig. 6). No similar situation is observed during the rest of the campaign. In Roma, Perrino et al. (2002) observed high levels of $NH_3$ at curbside sites with a diurnal profile clearly influenced by traffic emissions. However, due to the combined action of dry deposition, dilution after emissions as well as the conversion into particulate $NH_4^+$ (with sulfates and/or nitrates), these concentrations were severely reduced at the urban background scale (about a factor of 5) and the traffic profile type had disappeared. As a result, our urban background conditions may have prevented us from accurately assessing the potential impact of traffic emissions on ambient $NH_3$ concentrations. Investigating the $NH_3$ diurnal variability at the SIRTA site, Petit et al. (2015) noticed a bimodal traffic-like variation but only during spring and not during summer and winter, suggesting that these variations may be related to processes other than traffic.

### Influence of agricultural $NH_3$

As previously mentioned, $NH_3$ is emitted by both agricultural and non-agricultural sources. The former clearly dominates at the national scale, as well as at the scale of the Paris region (which includes the rural areas surrounding Paris), while the latter dominates at the scale of the city itself (which includes only urban areas). Considering the role of $NH_3$ in the formation of $NH_4NO_3$ and the important contribution of this aerosol compound to the $PM_{2.5}$ pollution in Paris, it is of major importance to assess the relative contribution of both types of sources to the $NH_3$ urban background in the city. Answering that question would ideally require additional $NH_3$ observations in Paris and its surroundings in order to quantify the increment associated to local sources. Without such observations, it is not possible to quantitatively investigate the $NH_3$ budget in Paris.

However, based on the available observations, we argue in this section that among all $NH_3$ emission sources, agriculture is probably the main driver of the day-to-day variability

of $NH_3$ concentrations in Paris during the time of the campaign (from spring to autumn) (in conjunction with the thermodynamic equilibrium that drives the partitioning between the gas and aerosol phases).

This is mainly supported by the $NH_3$ (and $TNH_3$) seasonal variations. Although incomplete (due to missing observations in winter and early spring), the $NH_3$ seasonal pattern shows a maximum in spring and early summer, moderate concentrations in late summer, and a minimum in autumn. Such a seasonal pattern has been already reported in several studies (e.g., Reche et al., 2012; Skjøth et al., 2011). A roughly similar variability is expected for the fertilizer applications, yet this emission source represents around 40 % of the total agricultural source at the national scale, and this contribution appears even higher around the Paris region (Hamaoui-Laguel et al., 2014; see in particular their Fig. 2a and b). The observed increase of $NH_3$ with temperature is also compatible with this source, as increased temperature favors fertilizer evaporation (e.g., Hamaoui-Laguel et al., 2014). Conversely, none of the non-agricultural emission sources are expected to be particularly intense during this time of the year. This was discussed for traffic-related emissions in the last section. Some $NH_3$ may also be emitted by biomass burning (for residential heating) but these emissions are, in any case, low in spring and summer. Emissions from sewage and waste disposal as well as emissions from other biological sources may also contribute to $NH_3$ levels. Interestingly, these latter sources may be influenced by temperature, as are the $NH_3$ concentrations measured in Paris (see Fig. 4). However, if they dominate, one would not expect such a large difference in concentrations between late May, early June and August (when temperatures were comparable). Additionally, in this case, one would also expect higher $NH_3$ concentrations during stagnant conditions, which is in contradiction with the low correlation between BC and $NH_3$ (given that such stagnant conditions lead to an accumulation of BC). The $NH_3$ diurnal profile shows very limited variations along the day, which is consistent with the idea of a strong $NH_3$ background originating from agricultural sources around the Paris region. All these elements thus suggest that the agricultural source (and more precisely the fertilizer application) drives a larger part of the $NH_3$ day-to-day variability in Paris than the other emission sources.

**Geographical origin of the highest $NH_3$ episodes**

In this section, we investigate the geographical origin of the air masses associated with elevated $NH_3$ episodes. Back trajectories during the 10 days of highest $NH_3$ concentrations (daily averages above 9.2 ppb, the 95th percentile of all daily values) are presented in Fig. 7a. Most $NH_3$ episodes are associated with moderate winds at altitude (particles being released at 500 m a.g.l. in FLEXTRA simulations), air masses at D-1 (1 day before reaching Paris) being located in a radius of 50–400 km from Paris. A noticeable exception is found on 9 July in the morning (around 06:00 UTC) when the wind suddenly changes direction (from southeast to southwest) and speed (getting much stronger, with air masses originating from Spain at D-1) while $NH_3$ concentrations increase. Interestingly, some of the highest $NH_3$ episodes (e.g., 10 July) are associated with oceanic air masses (excepted to be relatively clean) that have spent only a limited time over land, which suggests the presence of intense $NH_3$ emissions in the corresponding regions (Normandy). The trajectory analysis suggests that air masses with high $NH_3$ concentrations do not appear to originate from a particular geographical region. Instead, the highest episodes appear linked to more diffuse $NH_3$ emissions in the northern part of France, associated with anticyclonic conditions with high temperature and moderate winds. This is in accordance with Petit et al. (2015) that suggest, based on $NH_3$ measurements at the SIRTA suburban site (southwest of Paris), a diffuse regional $NH_3$ source, in particular during summer (in spring, some high $NH_3$ episodes associated to east/northeast/southeast winds are also noticed, but without any clear pattern).

#### 4.2.2 Model results

As shown in Fig. 2, $NH_3$ concentrations are significantly underestimated by the CHIMERE model with a NMB of −75 % (see statistical results in Table 2). This negative bias affects not only the intense peaks but also the baseline concentrations. In their evaluation of the CALIOPE-EU modeling system, Pay et al. (2012) reviewed the statistical results of various regional models over Europe (during a whole year for most models). As our study does not cover a whole year, statistical results are not directly comparable, but figures still shed light on the relative performance of our CHIMERE simulation. The negative bias in our study is in the range of those reported by Pay et al. (2012) where NMB varied from −82 to −15 %. Our RMSE (3.9 ppb) is among the best values reported by Pay et al. (2012) (1.6 ppb for the CALIOPE-EU model and 7.6–10.6 ppb for the six other models), as well as the correlation (0.42 vs. 0.05–0.56). Nevertheless, the CHIMERE model dramatically fails to reproduce the strong spring and summer episodes (and consequently the seasonal variation) during which negative biases on daily concentrations can exceed a factor of 10, despite a monthly distribution of emissions peaking between March and May (spring fertilizer application).

The similar results obtained in the MOD and MOD-noIDF cases indicate that most of the simulated $NH_3$ originates from outside the region of Paris. Concentration maps show that simulated $NH_3$ concentrations closely follow the spatial distribution of emissions, with maximum levels over Brittany, northern France, and Benelux. Due to both dilution and deposition, $NH_3$ concentrations quickly decrease with distance from these source regions. However, the simulated $NH_3$ lifetime appears high enough to allow imports over the region of Paris. As an illustration, highest simulated concentrations

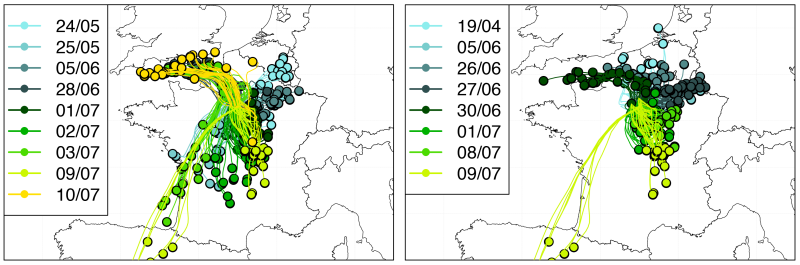


**Figure 7.** Back trajectories at D-1 (1 day before reaching Paris) associated with highest **(a)** $NH_3$ (left panel) and **(b)** $HNO_3$ (right panel) episodes (highest episodes being selected according to daily concentrations above the 97th percentile of all daily measurements, i.e., 9.2 and 0.9 ppb for $NH_3$ and $HNO_3$, respectively). For clarity, only back trajectories of seven particles around the center of Paris are plotted, each 6 h (i.e., 28 back trajectories per day).

in the city (4.5 ppb, the 29 April) result from the advection of air masses from eastern Brittany and southwest during the month of maximum emissions (according to monthly factors applied to emissions).

Comparing observations and model results at the MONTSOURIS meteorological station, a negative bias for temperature (−1.6 °C) and a positive bias for RH (+5.9 % in absolute) (see Sect. S2 in the Supplement) is noted. This favors the formation of $NH_4^+$ and thus decreases gaseous $NH_3$ in $TNH_3$. However, correcting these errors in the ISORROPIA model (i.e., replacing the simulated temperature and RH values with measured values, without modifying $TNH_3$, $TNO_3$, and TS concentrations) does not fill the gap with observations (the average $NH_3$ concentrations increasing by only 7 % on average). Errors may be larger close to the deliquescence point where the influence of RH is stronger. The deliquescent RH (DRH) of $NH_4NO_3$ and $(NH_4)_2SO_4$ at 298 K are 61.8 and 79.9 %, respectively (Seinfeld and Pandis, 2006). A mixture of both salts will have a DRH between these two extreme values. Focusing on days when RH ranges between 60 and 80 % (i.e., close to the deliquescent point of the mixture), the average $NH_3$ increase is even lower (6 %). It reaches 14 % when considering RH between 60 and 65 %. In any case, the impact remains limited. As shown in Fig. 5, the fraction of $NH_3$ in $TNH_3$ simulated by CHIMERE is highly variable, ranging from less than 5 % to about 90 %, in contradiction with observations which show a clear gas-phase reservoir during spring and summer (at around 60–100 %). The already mentioned overestimation of $SO_4^{2-}$ in CHIMERE (see Sect. 4.1) may directly reduce the amount of $NH_3$ available in the gas phase. However, the bias on $TNH_3$ is only reduced to −56 % (against −76 % for $NH_3$ alone), which indicates that only a minor part of the negative bias on $NH_3$ can be explained by an erroneous partitioning between both gas and aerosol phases (including errors related to $SO_4^{2-}$).

Although not likely the main $NH_3$ source (see Sect. "Influence of agricultural $NH_3$"), the traffic can also contribute to the $NH_3$ urban background levels in Paris. However, in the TNO-MP inventory, these traffic emissions are missing in the Paris region (but not outside this region) (see Table S3 in the Supplement), which may induce an underestimation of modeled $NH_3$ concentrations. The contribution of traffic to ambient $NH_3$ levels in urban environments is highly variable from one city to another, as illustrated by the $NH_3$ / ($NH_3$+$NO_x$) emission molar ratios that range from a few percent (Yao et al., 2013) to a few tens of percent (Bishop et al., 2010), which are due to differences in the vehicle fleet (Carslaw and Rhys-Tyler, 2013). Several sensitivity tests were performed with added $NH_3$ traffic emissions, derived from the $NO_x$ traffic emissions with $NH_3$ / ($NH_3$+$NO_x$) conversion factors in the range of the values given in the literature: 1, 6, 12, and 18 % (not shown). Such additional emissions reduce the bias, but do not improve the correlation between model and measurements. In particular, they induce a clear increase of $NH_3$ concentrations during the morning and evening rush hours, which is not in agreement with the observed diurnal profile. These results thus prevent us from concluding on the importance of these traffic emissions on $NH_3$ urban background levels.

A large part of the model errors probably arises from the representation of $NH_3$ air–surface exchanges (agricultural emissions and deposition) in the CHIMERE model. This representation is by far too simplistic in several respects: (i) the parameterization of $NH_3$ dry deposition is uni-directional and does not take into account the compensation with emissions; (ii) the agricultural emissions are temporally disaggregated based on monthly, day-of-the-week, and diurnal factors without taking into account any environmental factor (e.g., air temperature, soil moisture, agricultural practices) known to influence some $NH_3$ emissions (e.g., the volatilization of fertilizers). This likely explains the much lower $NH_3$-temperature correlation obtained in the model in comparison with observations ($r = 0.52$ against 0.72 in observations), as illustrated in Fig. 4. In light of our comparison, the parameterization of the $NH_3$ emissions in CHIMERE cannot represent the high spatiotemporal variability of $NH_3$ concentrations, and in particular fails in reproducing the large $NH_3$ peak values observed during the campaign. Indeed, these emissions result from very complex mechanisms in which

numerous environmental parameters are involved, including the amount of nitrogen fertilizers used over the land; temperature, moisture, and pH of the soil; the amount of soluble carbon; the soil disturbance and compaction; and fertilization methods (Ma et al., 2010, and references therein). More elaborated parameterizations of $NH_3$ bi-directional fluxes have been proposed to better handle emission and deposition processes in CTMs (Massad et al., 2010; Zhang et al., 2010; Pleim et al., 2013). Hamaoui-Laguel et al. (2014) have simulated more realistic $NH_3$ emissions over France during the spring 2007 by combining the one-dimensional mechanistic model VOLT'AIR (Garcia et al., 2011; Génermont and Cellier, 1997) with agricultural practice and soil data. They have shown a spatial variability of $NH_3$ emissions mainly driven by the soil pH and the types and rates of fertilization, while the temporal variability was rather driven by meteorological conditions and fertilization dates. Compared to the EMEP inventory (quite similar to TNO-MP for $NH_3$ emissions), the emissions computed with the VOLT'AIR mechanism appear lower over Brittany (in the west of France) and higher over the north of France (around a factor of 2–3). This would suggest a possible underestimation of agricultural $NH_3$ emissions close to the Paris region.

Dry deposition of $NH_3$ and wet deposition of $NH_4^+$ represent the two major sinks for $NH_3$ and $NH_4^+$, respectively; the first is dominant near emission sources whereas the second dominates at a larger scale (Asman et al., 1998). Uncertainties in the parameterization of both dry and wet deposition in the CHIMERE model may also partly explain the $NH_3$ underestimation. Results from the MOD-nodep sensitivity test (with no $NH_3$ dry deposition) allow assessing an upper bound of uncertainties related to dry deposition. On average, more than half of the $NH_3$ reaching Paris is deposited in the MOD case, as illustrated by the increase of $NH_3$ concentrations by a factor of 2.2 when deposition is removed. The diurnal profile indicates that deposition in CHIMERE more strongly affects nighttime concentrations, likely due to the shallow boundary layer. Daytime concentrations are also affected but approximately 2 times less than nighttime ones. Note that typical deposition velocities simulated by CHIMERE are around $0.3\,cm\,s^{-1}$, although it can substantially vary in time and space. Despite the unrealistic character of this sensitivity test (dry deposition being one of the dominant $NH_3$ sinks), this appears not sufficient to increase concentrations towards observed ambient levels (NMB of $-46\,\%$). Thus, deposition does not appear as the major source of error in the CHIMERE simulated $NH_3$.

#### 4.2.3 Conclusions on ammonia

Our $NH_3$ urban background measurements in Paris have highlighted several intense episodes in late spring and early summer. These episodes occur during anticyclonic conditions with high temperature, expected high agricultural emissions and moderate winds enabling an accumulation of $NH_3$ and a subsequent advection over the city. We argued that the observed $NH_3$ seasonal pattern supports the idea of a $NH_3$ day-to-day variability mainly driven by the agricultural source, in association with the thermodynamic equilibrium controlling the gas–aerosol partitioning.

CHIMERE simulations show a significant negative bias for $NH_3$, both for the baseline concentrations and the intense episodes. Errors in the partitioning of $TNH_3$ between the gas and aerosol phases (due to errors in modeled $SO_4^{2-}$, $NO_3^-$, or local meteorology) as well as uncertainties for deposition can only explain a minor part of the bias. Thus, the simulated $NH_3$ concentrations appear mainly affected by uncertainties in emissions, and in particular the lack of dynamical treatment of agricultural emissions as a function of environmental factors (temperature, etc.) in the CHIMERE model (the annual total emissions being simply disaggregated with a monthly profile).

### 4.3 Nitric acid

#### 4.3.1 Temporal variability

Daily concentrations and the diurnal profile of $HNO_3$ are shown in Fig. 2. Over the whole period, the average $HNO_3$ concentration is 0.25 ppb. Several moderate episodes are observed in spring and early summer, with daily concentrations up to 1.2 ppb at the beginning of July. This leads to a seasonal pattern characterized by higher values in spring/summer compared to autumn/winter. Such temporal variations are expected in urban environments close to $NO_x$ emissions due to both the higher OH triggered $HNO_3$ production in summer and the higher temperatures (as well as the lower RH) that diminish its condensation into particulate $NO_3^-$. They are also consistent with those found in other urban studies (Cadle et al., 1982; Cadle, 1985, in Warren, Michigan, USA; Solomon et al., 1992, in Los Angeles, California, USA; Perrino et al., 2002, in Roma, Italy).

In Paris, the highest $HNO_3$ episodes are associated with high temperatures and low-to-moderate wind speeds at the ground (see Fig. 7b). These conditions increase the atmospheric stratification and the residence time of $NO_x$ emissions over the agglomeration and allow for more efficient $HNO_3$ formation via the $NO_2$+OH reaction. This is confirmed by the fact that many $HNO_3$ peaks follow BC episodes; these episodes are often due to stagnant conditions allowing the accumulation of the BC emitted by the traffic.

This is illustrated during the first days of June in Fig. 8. 1 June is characterized by low wind speed but cloudy conditions that decrease the photooxidation rate of $NO_x$. During the next 2 days, stronger winds (above $3\,m\,s^{-1}$) and increasing temperatures are observed, associated with a moderate increase of $HNO_3$ concentrations. A much larger increase in $HNO_3$ concentrations is observed on 4 and 5 June concomitantly with high temperatures (up to 30 °C) and slow winds. Such stagnant conditions during the night allow the accumu-

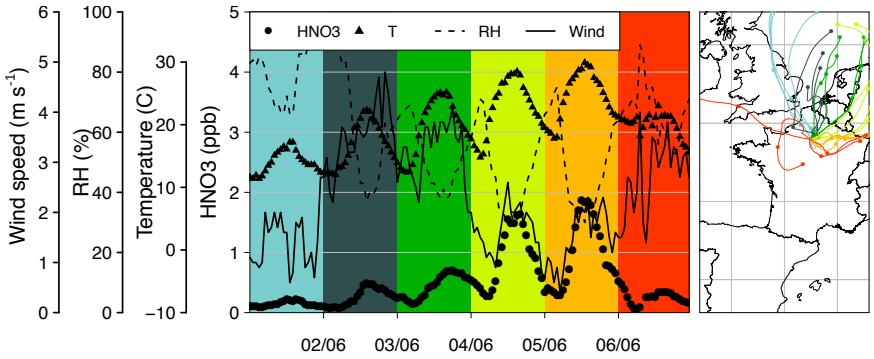


**Figure 8.** Hourly concentrations of $HNO_3$ at LHVP and wind speed, RH and temperature during early June 2010 (left panel), and associated 48 h back trajectories (one point every 24 h) colored by the day of arrival (i.e., red is for 6 June).

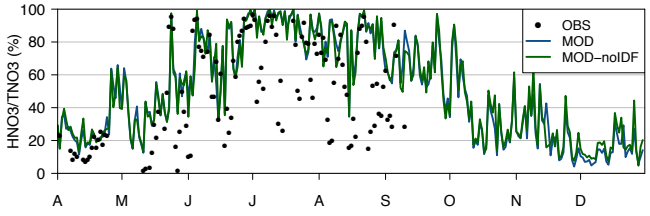


**Figure 9.** Daily $HNO_3$ / $TNO_3$ ratios.

lation of $NO_2$, as shown by the $NO_2$ measurements at an AIRPARIF station located right next to the LHVP site (not shown). In the early morning of 4 (5) of June, $NO_2$ concentrations reach 83 (110) ppb and fall below 20 ppb during the afternoon. As for $NH_3$, no additional $HNO_3$ measurements are available upwind of Paris, which prevents us from quantitatively assessing the importance of local formation vs. imports. However, this specific situation of early June supports the idea of a strong local formation of $HNO_3$. Some $HNO_3$ is also probably (slowly) advected by northeasterly winds but the strong photochemically driven diurnal variation observed during these days (where concentrations reach 1.5 ppb in the afternoon) suggests that this contribution is minor in comparison to the local formation. The episode ends concomitantly with a significant decrease in temperature and an increase in wind speed (thus favoring the dispersion).

The diurnal profile shows maximum $HNO_3$ concentrations in the afternoon at around 14:00–18:00 UTC (Fig. 2). On average, the ratio between daytime and nighttime $HNO_3$ concentrations is close to a factor of 2 (despite the development of the convective boundary layer in the afternoon). A slight decrease of $HNO_3$ is found at around 06:00 UTC, which may be explained by dew formation processes that allows the absorption of water-soluble gases such as $HNO_3$ (Mulawa et al., 1986; Parmar et al., 2001; Pierson et al., 1988), although no data are available to address this hypothesis.

$HNO_3$ accounts for 51 % of $TNO_3$ on average (Fig. 9) but this fraction appears highly variable. The lowest $HNO_3$ / $TNO_3$ ratios (a few %) are observed during cold days in mid-May when daily temperatures fall below 8 °C (see Fig. S2 in the Supplement), while the highest ratios occur during early summer, with values up to 96 %. The correlation between the $HNO_3$ / $TNO_3$ ratio and the temperature is 0.82, which illustrates the impact of temperature on the thermodynamic equilibrium.

Despite rather high temperatures, low ratios (below 40 %) are also observed on specific periods during summer, particularly in August. Such a pattern may be due to higher measurement uncertainties occurring for low $TNO_3$ concentrations, closer to the detection limit (roughly around 0.1 ppb for $HNO_3$). In August, ratio values below 40 % indeed correspond to $HNO_3$ and $TNO_3$ concentrations below 0.2 and 0.7 ppb, respectively.

### 4.3.2 Model results

$HNO_3$ concentrations are significantly overestimated by CHIMERE, with a NMB of +195 % and an NRMSE of 320 %, especially at midday when the bias can reach a factor of 4 (as illustrated by the diurnal profile in Fig. 2). The correlation is moderate ($r = 0.56$) when considering hourly concentrations but is slightly higher with daily values ($r = 0.68$).

Several uncertainties may explain the discrepancies between observed and simulated $HNO_3$ concentrations: (i) uncertainties in $NO_x$ emissions at both local and regional scales, (ii) uncertainties in the thermodynamic equilibrium (i.e., the errors on either the other inorganic compounds or the ISORROPIA model itself; Fountoukis and Nenes, 2007) that determine the distribution between gas and aerosol phases, (iii) uncertainties in the OH concentrations that directly influence the conversion of $NO_2$ into $HNO_3$, (iv) uncertainties in the $HNO_3$ deposition, and (v) errors in the transport. At the European scale, uncertainties in $NO_x$ emissions are estimated to be around 30 % (Deguillaume et al., 2007; Konovalov et al., 2006) and are thus much lower than the errors obtained for modeled $HNO_3$. Over the Paris agglomeration, $NO_x$ emissions from the TNO-MP inventory

used in our model have been evaluated during summer 2009 based on aircraft measurements in the Paris plume, showing no significant bias (Petetin et al., 2015). Dry deposition plays an important role in the $HNO_3$ budget, and corresponding parameterizations incorporated in the CHIMERE model have been poorly evaluated so far. In fact, an underestimated deposition rate in CHIMERE may partly explain the positive bias on $HNO_3$. In CHIMERE, $HNO_3$ deposition velocities are typically below $1.5\,cm\,s^{-1}$, which appears on the lower end of the values reported in the literature (Brook et al., 1999). However, due to a lack of appropriate data, this hypothesis remains difficult to assess. Finally, significant errors in the transport pattern remain unlikely given the good correlations obtained on nitrates between the observations and the model. The next subsections aim to investigate in more details the uncertainties related to the simulated thermodynamic equilibrium and OH radical.

### Uncertainties associated with thermodynamic equilibrium

Bias and RMSE are much lower for $TNO_3$ (NMB of +71 %, NRMSE of 121 %) than for $HNO_3$, because the CHIMERE model overestimates the $HNO_3$ / $TNO_3$ fraction (on average 68 % for the model against 51 % observed from experimental data during the period with available observations of $NO_3^-$ and $HNO_3$). Partitioning errors may derive from uncertainties in the ISORROPIA thermodynamic model (e.g., model formulation, chemical compounds included, activity coefficients treatment) or in its input data. Apart from CHIMERE, the ISORROPIA model is used in many other CTMs, including LOTOS-EUROS (Schaap et al., 2008), REM-CALGRID (Stern, 2003), CAMx, FARM, or CMAQ. It has been validated in various studies based on comparisons with observations (Moya et al., 2001) or against other widely used thermodynamic models (Nenes et al., 1999; Carnevale et al., 2012). From these studies, several uncertainty sources emerge: The hypothesis (used in ISORROPIA) of an instantaneous equilibrium between gas and aerosol phases (Aan de Brugh et al., 2012) is without incidence for our study, since the CHIMERE model treats the evolution of inorganic compounds concentrations through a dynamic approach (see Sect. 3.1). The absence of sodium, chloride, and other crustal species ($Ca^{2+}$, $K^+$, $Mg^{2+}$) in our simulations may also induce errors in the system (Fountoukis and Nenes, 2007), but the contribution of this crustal material remains low in the Paris region, about 5 % on average from 1 April to 10 September (with a percentile 95 at 13 %), as previously noted by Bressi et al. (2013). This low contribution of crustal species is confirmed by the ion balance obtained when considering only ammonium, nitrate, and sulfate: $NH_4^+$ vs. $NO_3^- + 2SO_4^{2-}$ (all species expressed in ppb) gives a slope of 1.01, a $y$ intercept of $-0.20$ and a correlation $r^2 = 0.97$ (see Fig. S1 in the Supplement).

Therefore, errors in the modeled partitioning are most likely due to errors in the other inorganic compounds involved in the $HNO_3$–$NO_3^-$ equilibrium. In particular, the large negative bias on $NH_3$ described in Sect. 4.2 can potentially lead to an underestimation of the $NH_4NO_3$ formation and consequently to an overestimation of $HNO_3$. A sensitivity test has been performed for that purpose with the ISORROPIA model running alone (i.e., not coupled with CHIMERE) fed by the concentrations previously obtained with CHIMERE for inorganic species except for $NH_3$ for which measurements were taken into account. This approach changes $HNO_3$ concentrations, for instance a decrease of 29 % in May. However, the significant positive bias in $HNO_3$ in summer persists ($HNO_3$ concentrations decrease by only 11 % between June and August), mainly because during summer $NH_4NO_3$ concentrations are very small and $HNO_3$ is the major $TNO_3$ component due to the relatively high temperatures.

### Uncertainties associated with OH concentrations

Assuming that (i) the $NO_2$+OH reaction is likely the dominant direct homogeneous pathway for $HNO_3$ formation during the summertime period, (ii) a significant bias is observed for modeled $TNO_3$, and (iii) the maximum discrepancies between measurements and modeled $HNO_3$ are found during midday, uncertainties in simulated OH could explain a substantial part of the errors on $HNO_3$. Many studies have attempted to quantify uncertainties in sources and sinks of OH, traditionally through the direct comparison between observations and calculations from detailed chemistry schemes (in box models) fed by ancillary observations of various parameters (e.g., VOC, $NO_x$, and $O_3$ concentrations, photolysis rates). In such exercises, uncertainties in daytime OH concentrations usually remain below a factor of 2 (see Kanaya et al., 2007, for a review, where the ratio of simulated to observed daytime OH concentrations ranges between 0.5 and 1.5). During summertime, Michoud et al. (2012) observed a very low overestimation (5 %) of simulated OH concentrations in Paris using the Master Chemical Mechanism (MCM) chemistry scheme. However, these results need to be taken as a lower end of OH uncertainties in CTMs where constraints are applied on neither long-lived compounds nor photolysis rates. This is especially true in an urban environment where concentration gradients of compounds impacting on the OH budget are strong.

In order to assess the influence of OH on $HNO_3$ formation, a sensitivity test (hereafter designated by MOD-OHx0.5) has been performed over a period of 35 days in June/early July by artificially reducing OH concentrations. This is technically performed by decreasing by a factor of 2 the $HO_x$ ($HO_x = OH + HO_2 + RO_2$) formation yields (i.e., the stoichiometric coefficient) in several (initiation) reactions, including the photolytic destruction of $O_3$, formaldehyde, acetaldehyde, glyoxal, and methyl glyoxal. OH and $HNO_3$ con-

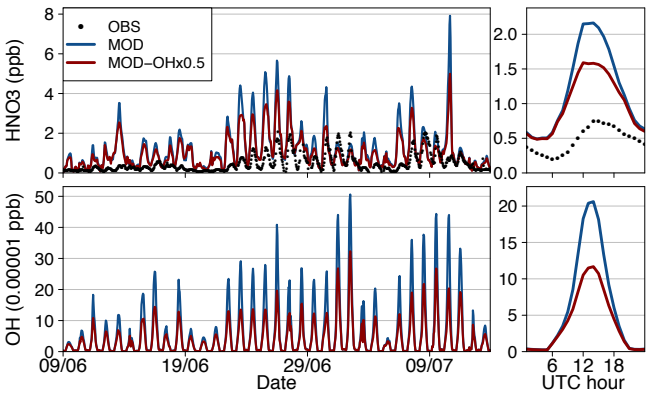


**Figure 10.** $HNO_3$ and OH hourly concentrations (left panel) and diurnal profiles (right panel) at the LHVP site.

centrations are then compared to the reference MOD case in Fig. 10. On average, concentrations of OH and $HNO_3$ are reduced by −36 and −16 %, respectively. The changes in $NO_x$ concentrations remain below 3 %, which means that only a minor fraction of $NO_x$ is oxidized within Paris. These decreases are even larger during midday when they reach −42 and −25 %, respectively. Over midday, the bias between measured and modeled $HNO_3$ is reduced to +113 % (compared to +154 % in the MOD case). Uncertainties in the OH radical may thus explain a significant part of the CHIMERE errors on $HNO_3$.

#### 4.3.3 Conclusions on $HNO_3$

$HNO_3$ concentrations experimentally determined in Paris show several intense peaks in late spring and early summer that coincide with high air temperatures and low to moderate wind speeds. The share between local production and imports remains difficult to assess precisely, but local $HNO_3$ may represent a major source during some specific time-limited episodes. However, uncertainties persist, and the CHIMERE errors are unfortunately too high to help the investigation of $HNO_3$ origin. Indeed, the model largely overestimates measured $HNO_3$ concentrations, approximately by a factor 3, with the highest biases observed in the middle of the day. The negative bias between measured and modeled $NH_3$ explains a part of the poor model performance for $HNO_3$ but still fails to explain errors during summertime when $TNO_3$ is mostly in the gas phase. Uncertainties in $NO_x$ emissions are much lower than errors obtained on $HNO_3$ and cannot explain the results of the model. Uncertainties related to the dry deposition of $HNO_3$ cannot be assessed and could contribute to the discrepancies given by the model. Finally, a too large $NO_2$-to-$HNO_3$ conversion through an overestimation of the OH radical concentrations in CHIMERE could also contribute to the large modeled overestimation of $HNO_3$ formation. Indeed, due to the absence of appropriate validation, uncertainties in simulated OH still remain high in CHIMERE (probably more than a factor of 2) and reducing OH sources have shown to lead to a significant decrease in OH and $HNO_3$ concentrations, in particular during the afternoon when $NO_2$ photooxidation (as well as the $HNO_3$ bias) is at its maximum.

### 4.4 Aerosol nitrate formation

#### 4.4.1 Results of the CHIMERE simulations

Fine particulate pollution with high $NO_3^-$ contents in Paris consists of intense (up to 16 µg $m^{-3}$ in late spring) and time-limited (a few days) episodes associated with continental wind regimes. Very low levels of nitrate are observed during periods with marine (clean) air masses and during summertime (due to volatilization). Despite the large errors previously highlighted for both $NH_3$ and $HNO_3$, the CHIMERE model provides relatively good results for nitrate with a NMB of +19 % and a correlation of 0.81, but still with a large NRMSE (109 %). As previously mentioned, in the framework of the PARTICULES campaign, $PM_{2.5}$ chemical constituents have also been measured at three rural sites around the Paris region. Results have been analyzed in terms of local and imported contributions by Petetin et al. (2014) who found that imported sulfate was slightly underestimated by CHIMERE (−17 %) while the local production of sulfate was overestimated (+32 %), leading at the end to a moderate negative bias (−17 %). For nitrates, they found a similar but larger error compensation identified between imported and local production (bias of +63 and −109 %, respectively), leading to a bias in Paris of +23 %. More details can be found in Petetin et al. (2014) (e.g., statistical results in Table 7).

It is worth noting that the positive bias highlighted here on the urban background concentrations in Paris should partly originate from experimental (negative) artifacts. The model may underestimate $NO_3^-$ if the experimental data are corrected for semi-volatile losses. The semi-volatile particulate matter (SVPM) can be deduced from the difference between TEOM-FDMS and TEOM $PM_{2.5}$ concentrations. If we attribute all that SVPM to $NH_4NO_3$, the bias between measured and modeled $NO_3^-$ becomes −48 %. This corresponds to an upper bound of the bias since SVPM contains not only $NH_4NO_3$ but also semi-volatile organic aerosol (OA). Semi-volatile OA may contribute the most to SVPM, as suggested by the higher correlation of SVPM with OA in comparison with $NH_4NO_3$ (0.59 vs. 0.32).

In conclusion, the either positive or negative bias in simulated nitrates and ammonium remains relatively small in comparison with the biases reported previously for precursor species. Such a result is not intuitive and cannot be trivially explained. An interesting point to illustrate is the possible error compensation related to the saturation condition that needs to be achieved to allow the formation of nitrates. This condition is defined as (Ansari and Pandis, 1998)

$$[TNO_3]\,([TNH_3] - 2\,[TS]) > K, \quad (6)$$

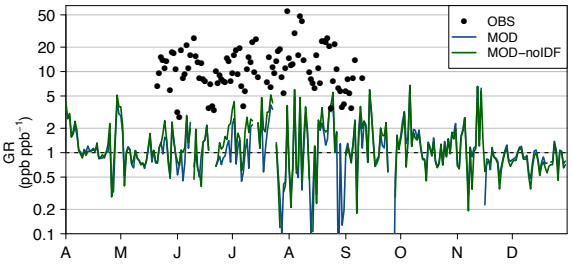


**Figure 11.** Observed and modeled daily GR.

with $K$ being the equilibrium constant that depends on various parameters, including temperature and RH. It is obvious here that the errors in $TNO_3$ and $TNH_3$ can partly compensate each other. On average, the left-hand term is 3.6 and 2.5 ppb$^2$ based on observations and simulation, respectively, which corresponds to a NMB of −31 %, thus much lower than the NMB affecting the different species (+71, −56 and +48 % for $TNO_3$, $TNH_3$, and TS). This result thus suggests that the formation of nitrates is slightly less thermodynamically favored in the model than in the reality, which would be consistent with a moderate negative bias in nitrates. Due to possible artifacts, our data set does not allow a complete assessment of the nitrate formation. It would be useful in the near future to evaluate the CHIMERE model with artifact-free measurements (for instance with aerosol mass spectrometer or aerosol chemical speciation monitor).

#### 4.4.2 Gas ratio and limiting species for nitrate formation

The GR has been proposed to assess which species among $NH_3$ and $HNO_3$ is the limiting reactant for $NH_4NO_3$ formation (Ansari and Pandis, 1998). It is defined as follows (with concentrations expressed in ppb):

$$\mathrm{GR} = \frac{[\mathrm{TNH_3}] - 2\,[\mathrm{TS}]}{[\mathrm{TNO_3}]}. \quad (7)$$

GR values above 1 indicate a regime mainly limited by $HNO_3$ (i.e., $NH_3$-rich regime) in which there is enough $NH_3$ to neutralize both sulfate and nitrate. Conversely, a GR between 0 and 1 indicates that there is enough $NH_3$ to neutralize sulfate but not nitrate, while negative GR corresponds to a $NH_3$-poor regime in which $NH_3$ amounts are insufficient to neutralize even sulfate. Nonlinear PM responses to inorganic concentration changes are expected at GR near unity (Ansari and Pandis, 1998).

As shown on Fig. 11, daily GR measurements are available only from the end of May (no $NH_3$ observations before) until the beginning of September (no aerosol observations after). During that period, experimentally determined daily GR values are highly variable (ranging between 2.8 to 56.3) but always remain above unity (12.6 on average), thus indicating that a large amount of ammonia is available for neutralizing nitric acid.

Observed GR may be affected by negative artifacts of nitrate filter measurements (Sect. 2.1). If we assume here that all the SVPM is $NH_4NO_3$ (see Sect. 4.4.1), one can calculate an artifact-corrected GR with both evaporated $NH_4^+$ and $NO_3^-$ added to measured $TNH_3$ and $TNO_3$, respectively. Compared to the previous GR, the artifact-corrected GR is reduced to an average value of 7.3 (the median is 3.5), thus still well above 1. In addition, as noticeable amounts of OA are expected to be included in the evaporated portion, this artifact-corrected GR has to be considered as a lower estimate of the actual GR values. The nitrate formation in Paris thus appears mainly limited by $HNO_3$. Over Europe, Pay et al. (2012) have also observed GR above 1 in several regions (e.g., Switzerland, Italy, Austria, inland regions of Spain and Denmark; no data in France), but taking into account observations restricted to regional background stations (i.e., enriched by agriculture ($NH_3$) emissions instead of traffic ($NO_x$) emissions). In our study, we show that such a $NH_3$-rich regime is also observed within a large megacity like Paris. Considering the high $NO_x$ emissions in the Paris megacity, such a result is counterintuitive but may be explained (as previously mentioned in Sect. 4.3.2) by a too slow $NO_x$-to-$HNO_3$ conversion rate compared to the efficient dispersive conditions.

In the CHIMERE model, the negative bias for $TNH_3$ and the positive biases for $TNO_3$ and $SO_4^{2-}$ result in a significant underestimation of modeled GR. On average, the model simulates a GR slightly above unity (1.2). Daily values continuously alternate between the $NH_3$-rich and $NH_3$-poor regimes with 48 % of simulated daily values remaining below unity (47 % considering the whole data set). The diurnal profile given by CHIMERE indicates that the GR regime changes within a single day, the lowest GR values (below 1) being simulated at 12:00 UTC (between the maximum $TNO_3$ occurring at 08:00 UTC and the minimum $TNH_3$ simulated at 15:00 UTC). Therefore, due to significant errors in gaseous precursors (and to a lesser extent in sulfate), the CHIMERE model fails half of time at correctly simulating the $HNO_3$-limited regime for nitrate formation in Paris on a daily basis.

#### 4.4.3 Sensitivity to perturbations

The GR value alone does not allow predicting the sensitivity of nitrate formation with respect to changes in gas precursor concentrations. This is due to the inability of GR to take into account both the need for the atmosphere to be saturated with $NH_3$ and $HNO_3$ (which acts as a threshold effect; see formula 6 in Sect. 4.4.1) and the influence of temperature and RH. Additional information can be given by the sensitivity coefficient $S_x$ (Takahama et al., 2004) of nitrate formation, defined as

$$S_x = \frac{\Delta \mathrm{NO_3}}{\mathrm{NO_3}} \frac{x}{\Delta x}, \quad (8)$$

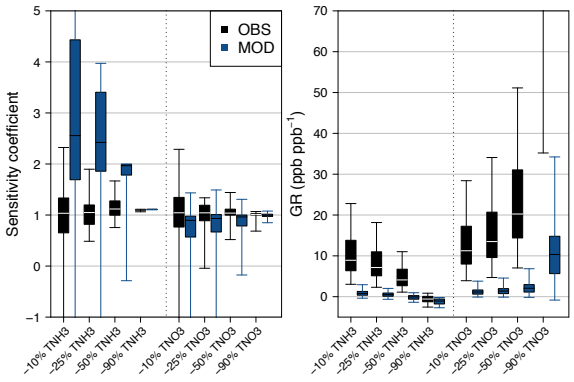


**Figure 12.** Sensitivity coefficient $S_x$ of nitrate formation due to different changes (−10, −25, −50, and −90 %) in $TNH_3$ and $TNO_3$ concentrations (left panel) and resulting GR (right panel) during the period from 15 May to 10 September 2010. Experimental data (OBS) are in black, modeled data (MOD) in blue. Box plots indicate 5th, 25th, 50th, 75th, and 95th percentiles.

where $\Delta NO_3$ refers to the change in nitrate concentrations obtained after a $\Delta x$ change of the parameter $x$ (e.g., temperature, RH, $TNH_3$, $TNO_3$, or TS).

The ISORROPIA thermodynamic model is used here to compute the sensitivity coefficient $S_x$ as a function of various decreases (−10, −25, −50, and −90 %) in $TNH_3$ and $TNO_3$ concentrations. This zero-dimension model requires fives inputs – temperature, RH, and $TNO_3$, $TNH_3$, and TS concentrations – and computes the gas–aerosol partitioning coefficient for $TNO_3$ and $TNH_3$ compounds. Also note that the analysis is local, as it is performed for the observed and simulated set of parameters at the urban background site. Decreasing the concentration of $TNO_3$ (or $TNH_3$) leads to a change in its partitioning between both the gas and aerosol phases. This change not only depends on the concentration of the family species which is altered but also on the value of all the other parameters of the system. Thus, the CHIMERE errors in the different input parameters propagate to the gas–aerosol partitioning coefficient, which can potentially lead to an erroneous sensitivity of nitrates to a change in $TNO_3$ or $TNH_3$. Calculations are performed for both the measurements and the model; i.e., all inputs are taken from the observations and the model, respectively, at the urban background site. In each case, the (observed or simulated) concentrations of $TNH_3$ or $TNO_3$ are decreased and the sensitivity coefficient is computed to quantify the impact of this change on the nitrate concentrations. Sensitivity coefficient results and corresponding GR are shown in Fig. 12.

For the experimental data, we do observe a quite similar sensitivity of nitrate formation for changes either in $TNH_3$ or in $TNO_3$ concentrations, with median sensitivity coefficients around 1 (i.e., close to a linear response). Considering the high GR values (except for the −50 and −90 % $TNH_3$ cases that lead to negative GR), such a result with similar responses to both precursors changes appears quite counterintuitive in light of the above definition of GR. However, first, the GR approach considers free $NH_3$, while the sensitivities are calculated with respect to total $NH_3$. Second, as already mentioned, the formation of nitrates requires the saturation condition to be achieved (see Eq. 6). So for large GR values, but small $TNO_3$ and free $NH_3$ values, nitrate formation will be sensitive to both $TNO_3$ and $TNH_3$. Note that the equilibrium constant $K$ (and thus the nitrate sensitivity) also depends on temperature and RH; this is illustrated in Fig. S6 in the Supplement where the same sensitivity tests are performed after decreasing the temperature by 10 °C and increasing the RH by 0.20 in observations, which leads to $S_{TNO_3}$ (still close to 1) much higher than $S_{TNH_3}$ (below 0.5 for −10 and −25 % of $TNH_3$), in accordance with the $NH_3$-rich regime given by GR.

The CHIMERE nitrate response to $TNO_3$ changes is approximately linear (i.e., $S_{TNO_3}$ close to 1), in reasonable agreement with observations. However, the model highly overestimates the sensitivity to $TNH_3$ changes, with median $S_{TNH_3}$ up to 2.5 for moderate $NH_3$ decreases while observations show (as for $TNO_3$ changes) a linear response to $TNH_3$ changes (i.e., $S_{TNH_3}$ around 1). The model is able to reproduce the observed response only when $NO_3^-$ formation is severely $NH_3$-limited (negative GR) and when the aerosol nitrate formation is prevented (which corresponds to the −90 % $TNH_3$ case).

These results have serious implications on the use of the CHIMERE model for emissions reduction scenarios. As $TNH_3$ concentrations are closely linked to $NH_3$ emissions, they show that the benefits (in terms of fine aerosol concentrations) of reducing these emissions would likely be overestimated by the model, in particular for moderate reductions (below −50 %). In addition, in terms of dynamical evaluation, changes in $NH_3$ emissions in the next years may potentially degrade the CHIMERE performance on the simulation of $NH_4NO_3$ in Paris if the issues raised here are not addressed. This is an important conclusion for the use of the CHIMERE model (in that configuration and input data).

## 5 Conclusions

Ammonium nitrate is a major contributor to the fine particulate pollution in Europe, and a better characterization of its formation regime and variability (controlled by the availability of its gaseous precursors, $NH_3$ and $HNO_3$) is thus mandatory for setting up relevant PM control strategies.

In this study, long-term measurements of inorganic compounds in both gaseous ($NH_3$, $HNO_3$, $SO_2$) and aerosol ($NH_4^+$, $NO_3^-$, $SO_4^{2-}$) fractions have been used to assess the $NO_3^-$ formation regime in the Paris megacity over several months covering the spring/summer period of 2010. High episodes of $NH_3$ (up to 12 ppb on daily average) were observed during late spring and early summer. Considering both the seasonal and diurnal variations, these observations

suggest that agricultural activities are a major driver of the $NH_3$ day-to-day variability within the Paris megacity. Rather low $HNO_3$ concentrations were measured (below 1.5 ppb on daily average), despite the large amounts of gas precursors ($NO_x$) emitted by the traffic in the city of Paris. Some elevated $HNO_3$ episodes were observed during anticyclonic conditions (high temperature, low-to-moderate wind) and suggest a substantial local formation from the $NO_x$ emitted within Paris. However, our data set does not allow quantitatively assessing the relative contributions of this local formation as compared to imports. These experimental results lead to a $NH_3$-rich regime in the Paris urban environment (as indicated by high GR values), as already observed in previous studies over Europe but only in rural areas (i.e., closer to agricultural activities). However, sensitivity tests with the ISORROPIA thermodynamic model indicate that, in the specific environment of Paris (in terms of RH, temperature and inorganic compounds concentrations), the $NO_3^-$ formation remains equally influenced by decreases of $TNH_3$ and $TNO_3$. Considering the size of the Paris megacity and the intensity of $NO_x$ emissions, one would have primarily expected higher $HNO_3$ and lower $NH_3$ in the Paris center. This work thus sheds a new light on the topical debate relative to the respective responsibility of traffic and agriculture in the formation of $NH_4NO_3$, by highlighting substantial amounts of agricultural $NH_3$ and relatively low concentrations of $HNO_3$ in the city.

This detailed experimental data set has also offered the opportunity to evaluate for the first time the ability of the CHIMERE chemistry-transport model to simulate the $NH_3$–$HNO_3$–$NO_3^-$ system. Comparison between measurements and model estimates have shown significant negative (−75 %) and positive (+195 %) biases for $NH_3$ and $HNO_3$, respectively. Several sensitivity tests have been performed in order to rank the uncertainty sources responsible for these biases. The difficulty of the CHIMERE model to match $NH_3$ observations is likely due primarily to erroneous agricultural emissions (in particular their spatiotemporal variability). By comparison, the contribution of $NH_3$ traffic emissions in the Paris agglomeration appears minor during the studied period but requires a more detailed quantification. Besides the (hardly quantifiable) uncertainties associated with dry deposition, errors in $HNO_3$ can probably be explained by the large uncertainties in OH concentrations, in particular during summertime, while the negative bias in $NH_3$ explains a noticeable portion of the $HNO_3$ overestimation during spring (by preventing $HNO_3$ conversion to $NO_3^-$).

The sensitivity of $NO_3^-$ formation as a function of decreasing concentrations of gas precursor have been investigated, highlighting a very high sensitivity to $NH_3$ changes in the model, in disagreement with observations that give a quasi linear response. Such results may have important implications on the use of CHIMERE for emission reduction scenarios (at least in the Paris region) by potentially overestimating the benefit of $NH_3$ emission reductions in terms of reductions of PM concentrations. The diagnostic evaluation led in this paper gives first results that need to be extended, notably with hourly artifact-free ($NH_4NO_3$) measurements during all seasons, in order to assess more precisely the $NO_3^-$ formation regime in the city of Paris. Additional work on uncertainty sources is also required to reduce the highlighted errors, in particular the $NH_3$ agricultural emissions and the OH uncertainties. The recent $NH_3$ measurements provided by IASI (Infrared Atmospheric Sounding Interferometer; Clarisse et al., 2009, 2010) may offer opportunities to better assess the spatial distribution of $NH_3$ emissions and help build more accurate emission inventories.

## Data availability

The data collected during the FRANCIPOL campaign are available upon request (Valérie Gros, valerie.gros@lsce.ipsl.fr), as well as the measurements performed during the PARTICULES campaign (Véronique Ghersi, veronique.ghersi@airparif.fr).

**The Supplement related to this article is available online at doi:10.5194/acp-16-10419-2016-supplement.**

*Acknowledgements.* This work is funded by a PhD DIM (domaine d'intérêt majeur) grant from the Île-de-France region. The PARTICULES project has been funded by the French state, the Île-de-France region, and the city of Paris. The FRANCIPOL projet has received funding from PRIMEQUAL, CNRS, CEA, the Île-de-France region, ACTRIS, and DIM R2DS. The authors gratefully acknowledge Jean-Charles Dupont and the SIRTA (sirta.ipsl.fr) for the useful boundary layer height data. The other meteorological data at Montsouris site have been kindly provided by METEO France.

Edited by: C. H. Song
Reviewed by: three anonymous referees

## References

Aan de Brugh, J. M. J., Henzing, J. S., Schaap, M., Morgan, W. T., van Heerwaarden, C. C., Weijers, E. P., Coe, H., and Krol, M. C.: Modelling the partitioning of ammonium nitrate in the convective boundary layer, Atmos. Chem. Phys., 12, 3005–3023, doi:10.5194/acp-12-3005-2012, 2012.

Airparif: Inventaire des émissions en Ile-de-France – Méthodologie et résultats – Année 2005, Technical report, available at: http://www.airparif.asso.fr/_pdf/publications/Rinventaire_2005_201004.pdf, 2010 (in French).

Airparif: Origine des particules en Ile-de-France, Technical report, available at: http://www.airparif.asso.fr/_pdf/publications/rapport-particules-110914.pdf, 2011 (in French).

Airparif: Source apportionment of airborne particles in the Ile-de-France region, Technical report, available at: http://www.airparif.asso.fr/_pdf/publications/rapport-particules-anglais-120829.pdf, 2012.

Ansari, A. S. and Pandis, S. N.: Response of Inorganic PM to Precursor Concentrations, Environ. Sci. Technol., 32, 2706–2714, doi:10.1021/es971130j, 1998.

Asman, W. A. H., Sutton, M. A., and Schjorring, J. K.: Ammonia: emission, atmospheric transport and deposition, New Phytol., 139, 27–48, doi:10.1046/j.1469-8137.1998.00180.x, 1998.

Baklanov, A., Lawrence, M., Pandis, S., Mahura, A., Finardi, S., Moussiopoulos, N., Beekmann, M., Laj, P., Gomes, L., Jaffrezo, J.-L., Borbon, A., Coll, I., Gros, V., Sciare, J., Kukkonen, J., Galmarini, S., Giorgi, F., Grimmond, S., Esau, I., Stohl, A., Denby, B., Wagner, T., Butler, T., Baltensperger, U., Builtjes, P., van den Hout, D., van der Gon, H. D., Collins, B., Schluenzen, H., Kulmala, M., Zilitinkevich, S., Sokhi, R., Friedrich, R., Theloke, J., Kummer, U., Jalkinen, L., Halenka, T., Wiedensholer, A., Pyle, J., and Rossow, W. B.: MEGAPOLI: concept of multi-scale modelling of megacity impact on air quality and climate, Adv. Sci. Res., 4, 115–120, doi:10.5194/asr-4-115-2010, 2010.

Bessagnet, B., Menut, L., Curci, G., Hodzic, A., Guillaume, B., Liousse, C., Moukhtar, S., Pun, B., Seigneur, C., and Schulz, M.: Regional modeling of carbonaceous aerosols over Europe – focus on secondary organic aerosols, J. Atmos. Chem., 61, 175–202, doi:10.1007/s10874-009-9129-2, 2009.

Bishop, G. A., Peddle, A. M., Stedman, D. H., and Zhan, T.: On-road emission measurements of reactive nitrogen compounds from three California cities., Environ. Sci. Technol., 44, 3616–3620, doi:10.1021/es903722p, 2010.

Blanchard, C. L. and Hidy, G. M.: Effects of changes in sulfate, ammonia, and nitric acid on particulate nitrate concentrations in the Southeastern United States, J. Air Waste Manage. Assoc., 53, 283–290, doi:10.1080/10473289.2003.10466152, 2003.

Bressi, M., Sciare, J., Ghersi, V., Bonnaire, N., Nicolas, J. B., Petit, J.-E., Moukhtar, S., Rosso, A., Mihalopoulos, N., and Féron, A.: A one-year comprehensive chemical characterisation of fine aerosol ($PM_{2.5}$) at urban, suburban and rural background sites in the region of Paris (France), Atmos. Chem. Phys., 13, 7825–7844, doi:10.5194/acp-13-7825-2013, 2013.

Brook, J. R., Zhang, L., Li, Y., and Johnson, D.: Description and evaluation of a model of deposition velocities for routine estimates of dry deposition over North America. Part II: review of past measurements and model results, Atmos. Environ., 33, 5053–5070, doi:10.1016/S1352-2310(99)00251-4, 1999.

Cadle, S., Countess, R., and Kelly, N.: Nitric acid and ammonia in urban and rural locations, Atmos. Environ., 16, 2501–2506, doi:10.1016/0004-6981(82)90141-X, 1982.

Cadle, S. H.: Seasonal variations in nitric acid, nitrate, strong aerosol acidity, and ammonia in an urban area, Atmos. Environ., 19, 181–188, doi:10.1016/0004-6981(85)90149-0, 1985.

Camargo, J. A. and Alonso, A.: Ecological and toxicological effects of inorganic nitrogen pollution in aquatic ecosystems: A global assessment., Environ. Int., 32, 831–849, doi:10.1016/j.envint.2006.05.002, 2006.

Carnevale, C., Finzi, G., Pisoni, E., Thunis, P., and Volta, M.: The impact of thermodynamic module in the CTM performances, Atmos. Environ., 61, 652–660, doi:10.1016/j.atmosenv.2012.06.058, 2012.

Carslaw, D. C. and Rhys-Tyler, G.: New insights from comprehensive on-road measurements of $NO_x$, $NO_2$ and $NH_3$ from vehicle emission remote sensing in London, UK, Atmos. Environ., 81, 339–347, doi:10.1016/j.atmosenv.2013.09.026, 2013.

Chow, J. C.: Health Effects of Fine Particulate Air Pollution: Lines that Connect, J. Air Waste Manage. Assoc., 56, 707–708, doi:10.1080/10473289.2006.10464484, 2006.

CITEPA: Inventaire des émissions de polluants atmosphériques et de gaz à effet de serre en France – Séries sectorielles et analyses étendues, 2013.

Clarisse, L., Clerbaux, C., Dentener, F., Hurtmans, D., and Coheur, P.-F.: Global ammonia distribution derived from infrared satellite observations, Nat. Geosci., 2, 479–483, doi:10.1038/ngeo551, 2009.

Clarisse, L., Shephard, M. W., Dentener, F., Hurtmans, D., Cady-Pereira, K., Karagulian, F., Van Damme, M., Clerbaux, C., and Coheur, P.-F.: Satellite monitoring of ammonia: A case study of the San Joaquin Valley, J. Geophys. Res., 115, D13302, doi:10.1029/2009JD013291, 2010.

Cowen, K., Sumner, A. L., Dinhal, A., Riggs, K., and Willenberg, Z.: Environmental Technology Verification Report, Mechatronics Instruments BV AiRRmonia Ammonia Analyzer, 2004.

Dall'Osto, M., Harrison, R. M., Coe, H., and Williams, P.: Real-time secondary aerosol formation during a fog event in London, Atmos. Chem. Phys., 9, 2459–2469, doi:10.5194/acp-9-2459-2009, 2009.

Davidson, C. I. and Wu, Y. L.: Dry deposition of particle and vapors, in: Acidic precipitation, vol. 3, edited by: Lindberg, S. E., Page, A. L., and Norton, S. A., Springer Verlag, New York, 103–216, 1990.

Deguillaume, L., Beekmann, M., and Menut, L.: Bayesian Monte Carlo analysis applied to regional-scale inverse emission modeling for reactive trace gases, J. Geophys. Res., 112, D02307, doi:10.1029/2006JD007518, 2007.

Denier van der Gon, H. A. C., Visschedijk, A., Van der Brugh, H., and Dröge, R.: A high resolution European emission database for the year 2005, a contribution to the UBA-project PAREST: Particle Reduction Strategies, TNO report TNO-034-UT-2010-01895_RPT-ML, Utrecht, 2010.

Denier van der Gon, H. A. C., Beevers, S., D'Allura, Al., Finardi, S., Honore, C., Kuenen, J., Perrussel, O., Radice, P., Theloke, J., Uzbasich, M., and Visschedijk, A.: Discrepancies Between Top-Down and Bottom-Up Emission Inventories of Megacities: The Causes and Relevance for Modeling Concentrations and Exposure, edited by: Steyn, D. G. and Castelli, S. T., NATO Science for Peace and Security Series C: Environmental Security, Vol. 4, Springer, ISBN 978-94-007-1358-1, 772 pp., 2011.

Dudhia, J.: A nonhydrostatic version of the Penn State/NCAR mesoscale model: validation tests and simulation of an Atlantic cyclone and cold front, Mon. Weather Rev., 121, 1493–1513, 1993.

Erisman, J. W., Van Pul, A., and Wyers, P.: Parametrization of surface resistance for the quantification of atmospheric deposition of acidifying pollutants and ozone, Atmos. Environ., 28, 2595–2607, doi:10.1016/1352-2310(94)90433-2, 1994.

Erisman, J. W., Otjes, R., Hensen, A., Jongejan, P., van den Bulk, P., Khlystov, A., Möls, H., and Slanina, S.: Instrument development and application in studies and monitoring of ambient

ammonia, Atmos. Environ., 35, 1913–1922, doi:10.1016/S1352-2310(00)00544-6, 2001.

Flechard, C. R., Nemitz, E., Smith, R. I., Fowler, D., Vermeulen, A. T., Bleeker, A., Erisman, J. W., Simpson, D., Zhang, L., Tang, Y. S., and Sutton, M. A.: Dry deposition of reactive nitrogen to European ecosystems: a comparison of inferential models across the NitroEurope network, Atmos. Chem. Phys., 11, 2703–2728, doi:10.5194/acp-11-2703-2011, 2011.

Folberth, G. A., Hauglustaine, D. A., Lathi'ere, J., and Brocheton, F.: Interactive chemistry in the Laboratoire de Météorologie Dynamique general circulation model: model description and impact analysis of biogenic hydrocarbons on tropospheric chemistry, Atmos. Chem. Phys., 6, 2273–2319, doi:10.5194/acp-6-2273-2006, 2006.

Fountoukis, C. and Nenes, A.: ISORROPIA II: a computationally efficient thermodynamic equilibrium model for $K^+$–$Ca^{2+}$–$Mg^{2+}$–$NH_4^+$–$Na^+$–$SO_4^{2-}$–$NO_3^-$–$Cl^-$–$H_2O$ aerosols, Atmos. Chem. Phys., 7, 4639–4659, doi:10.5194/acp-7-4639-2007, 2007.

Freney, E. J., Sellegri, K., Canonaco, F., Colomb, A., Borbon, A., Michoud, V., Doussin, J.-F., Crumeyrolle, S., Amarouche, N., Pichon, J.-M., Bourianne, T., Gomes, L., Prevot, A. S. H., Beekmann, M., and Schwarzenböeck, A.: Characterizing the impact of urban emissions on regional aerosol particles: airborne measurements during the MEGAPOLI experiment, Atmos. Chem. Phys., 14, 1397–1412, doi:10.5194/acp-14-1397-2014, 2014.

Garcia, L., Bedos, C., Génermont, S., Braud, I., and Cellier, P.: Assessing the ability of mechanistic volatilization models to simulate soil surface conditions: a study with the Volt'Air model, Sci. Total Environ., 409, 3980–3992, doi:10.1016/j.scitotenv.2011.05.003, 2011.

Génermont, S. and Cellier, P.: A mechanistic model for estimating ammonia volatilization from slurry applied to bare soil, Agr. Forest Meteorol., 88, 145–167, doi:10.1016/S0168-1923(97)00044-0, 1997.

Gong, L., Lewicki, R., Griffin, R. J., Flynn, J. H., Lefer, B. L., and Tittel, F. K.: Atmospheric ammonia measurements in Houston, TX using an external-cavity quantum cascade laser-based sensor, Atmos. Chem. Phys., 11, 9721–9733, doi:10.5194/acp-11-9721-2011, 2011.

Grantz, D. A., Garner, J. H. B., and Johnson, D. W.: Ecological effects of particulate matter, Environ. Int., 29, 213–39, doi:10.1016/S0160-4120(02)00181-2, 2003.

Guenther, A., Karl, T., Harley, P., Wiedinmyer, C., Palmer, P. I., and Geron, C.: Estimates of global terrestrial isoprene emissions using MEGAN (Model of Emissions of Gases and Aerosols from Nature), Atmos. Chem. Phys., 6, 3181–3210, doi:10.5194/acp-6-3181-2006, 2006.

Haeffelin, M., Angelini, F., Morille, Y., Martucci, G., Frey, S., Gobbi, G. P., Lolli, S., O'Dowd, C. D., Sauvage, L., Xueref-Rémy, I., Wastine, B., and Feist, D. G.: Evaluation of Mixing-Height Retrievals from Automatic Profiling Lidars and Ceilometers in View of Future Integrated Networks in Europe, Bound.-Lay. Meteorol., 143, 49–75, doi:10.1007/s10546-011-9643-z, 2012.

Hamaoui-Laguel, L., Meleux, F., Beekmann, M., Bessagnet, B., Génermont, S., Cellier, P., and Létinois, L.: Improving ammonia emissions in air quality modelling for France, Atmos. Environ., 92, 584–595, doi:10.1016/j.atmosenv.2012.08.002, 2014.

Hansen, M. C., Defries, R. S., Townshend, J. R. G., and Sohlberg, R.: Global land cover classification at 1 km spatial resolution using a classification tree approach, Int. J. Remote Sens., 21, 1331–1364, doi:10.1080/014311600210209, 2000.

Harrison, R. M. and Pio, C. A.: Size-differentiated composition of inorganic atmospheric aerosols of both marine and polluted continental origin, Atmos. Environ., 17, 1733–1738, doi:10.1016/0004-6981(83)90180-4, 1983.

Hass, H., Van Loon, M., Kessler, C., Stern, R., Matthijsen, J., Sauter, F., Zlatev, Z., Langner, J., Foltescu, V., and Schaap, M.: Aerosol modelling: results and inercomparison from European regional scale modeling systems, Eurotrac-ISS, Garmisch Partenkirchen, Germany, 2003.

Hauglustaine, D. A.: Interactive chemistry in the Laboratoire de Météorologie Dynamique general circulation model: Description and background tropospheric chemistry evaluation, J. Geophys. Res., 109, D04314, doi:10.1029/2003JD003957, 2004.

Healy, R. M., Sciare, J., Poulain, L., Kamili, K., Merkel, M., Müller, T., Wiedensohler, A., Eckhardt, S., Stohl, A., Sarda-Estève, R., McGillicuddy, E., O'Connor, I. P., Sodeau, J. R., and Wenger, J. C.: Sources and mixing state of size-resolved elemental carbon particles in a European megacity: Paris, Atmos. Chem. Phys., 12, 1681–1700, doi:10.5194/acp-12-1681-2012, 2012.

IPCC: Climate Change 2013: The Physical Science Basis. Contribution of Working Group I to the Fifth Assessment Report of the Intergovernmental Panel on Climate Change, edited by: Stocker, T. F., Qin, D., Plattner, G.-K., Tignor, M., Allen, S. K., Boschung, J., Nauels, A., Xia, Y., Bex V., and Midgley, P. M., Cambridge University Press, Cambridge, United Kingdom and New York, NY, USA, 1535 pp., 2013.

Kanaya, Y., Cao, R., Akimoto, H., Fukuda, M., Komazaki, Y., Yokouchi, Y., Koike, M., Tanimoto, H., Takegawa, N., and Kondo, Y.: Urban photochemistry in central Tokyo: 1. Observed and modeled OH and $HO_2$ radical concentrations during the winter and summer of 2004, J. Geophys. Res., 112, D21312, doi:10.1029/2007JD008670, 2007.

Kean, A. J., Littlejohn, D., Ban-Weiss, G. A., Harley, R. A., Kirchstetter, T. W., and Lunden, M. M.: Trends in on-road vehicle emissions of ammonia, Atmos. Environ., 43, 1565–1570, doi:10.1016/j.atmosenv.2008.09.085, 2009.

Kim, Y., Couvidat, F., Sartelet, K., and Seigneur, C.: Comparison of different gas-phase mechanisms and aerosol modules for simulating particulate matter formation, J. Air Waste Manage. Assoc., 61, 1218–1226, 2011.

Konovalov, I. B., Beekmann, M., Richter, A., and Burrows, J. P.: Inverse modelling of the spatial distribution of NOx emissions on a continental scale using satellite data, Atmos. Chem. Phys., 6, 1747-1770, doi:10.5194/acp-6-1747-2006, 2006.

Kuenen, J. J. P., Denier van der Gon, H. A. C., Visschedijk, A., Van der Brugh, H., and Van Gijlswijk, R.: MACC European emission inventory for the years 2003–2007, TNO report TNO-060-UT-2011-00588, Utrecht, 2011.

Kuenen, J. J. P., Visschedijk, A. J. H., Jozwicka, M., and Denier van der Gon, H. A. C.: TNO-MACC_II emission inventory; a multi-year (2003–2009) consistent high-resolution European emission inventory for air quality modelling, Atmos. Chem. Phys., 14, 10963–10976, doi:10.5194/acp-14-10963-2014, 2014.

Lombardo, T., Gentaz, L., Verney-Carron, A., Chabas, A., Loisel, C., Neff, D., and Leroy, E.: Characterisation of complex al-

teration layers in medieval glasses, Corros. Sci., 72, 10–19, doi:10.1016/j.corsci.2013.02.004, 2013.

Ma, B. L., Wu, T. Y., Tremblay, N., Deen, W., McLaughlin, N. B., Morrison, M. J., and Stewart, G.: On-Farm Assessment of the Amount and Timing of Nitrogen Fertilizer on Ammonia Volatilization, Agron. J., 102, 134–144, doi:10.2134/agronj2009.0021, 2010.

Massad, R.-S., Nemitz, E., and Sutton, M. A.: Review and parameterisation of bi-directional ammonia exchange between vegetation and the atmosphere, Atmos. Chem. Phys., 10, 10359–10386, doi:10.5194/acp-10-10359-2010, 2010.

Mather, T. A., Allen, A. G., Davison, B. M., Pyle, D. M., Oppenheimer, C., and McGonigle, A. J. S.: Nitric acid from volcanoes, Earth Planet. Sci. Lett., 218, 17–30, doi:10.1016/S0012-821X(03)00640-X, 2004.

Matsumoto, K. and Tanaka, H.: Formation and dissociation of atmospheric particulate nitrate and chloride: An approach based on phase equilibrium, Atmos. Environ., 30, 639–648, doi:10.1016/1352-2310(95)00290-1, 1996.

Menut, L., Bessagnet, B., Khvorostyanov, D., Beekmann, M., Blond, N., Colette, A., Coll, I., Curci, G., Foret, G., Hodzic, A., Mailler, S., Meleux, F., Monge, J.-L., Pison, I., Siour, G., Turquety, S., Valari, M., Vautard, R., and Vivanco, M. G.: CHIMERE 2013: a model for regional atmospheric composition modelling, Geosci. Model Dev., 6, 981–1028, doi:10.5194/gmd-6-981-2013, 2013.

Michoud, V., Kukui, A., Camredon, M., Colomb, A., Borbon, A., Miet, K., Aumont, B., Beekmann, M., Durand-Jolibois, R., Perrier, S., Zapf, P., Siour, G., Ait-Helal, W., Locoge, N., Sauvage, S., Afif, C., Gros, V., Furger, M., Ancellet, G., and Doussin, J. F.: Radical budget analysis in a suburban European site during the MEGAPOLI summer field campaign, Atmos. Chem. Phys., 12, 11951–11974, doi:10.5194/acp-12-11951-2012, 2012.

Moya, M., Ansari, A. S., and Pandis, S. N.: Partitioning of nitrate and ammonium between the gas and particulate phases during the 1997 IMADA-AVER study in Mexico City, Atmos. Environ., 35, 1791–1804, doi:10.1016/S1352-2310(00)00292-2, 2001.

Mozurkewich, M.: The dissociation constant of ammonium nitrate and its dependence on temperature, relative humidity and particle size, Atmos. Environ., 27, 261–270, doi:10.1016/0960-1686(93)90356-4, 1993.

Mulawa, P. A., Cadle, S. H., Lipari, F., Ang, C. C., and Vandervennet, R.: Urban dew: Its composition and influence on dry deposition rates, Atmos. Environ., 20, 1389–1396, doi:10.1016/0004-6981(86)90009-0, 1986.

Nenes, A., Pandis, S., and Pilinis, C.: ISORROPIA?: A New Thermodynamic Equilibrium Model for Multiphase Multicomponent Inorganic Aerosols, Aquat. Geochem., 4, 123–152, 1998.

Nenes, A., Pandis, S. N., and Pilinis, C.: Continued development and testing of a new thermodynamic aerosol module for urban and regional air quality models, Atmos. Environ., 33, 1553–1560, doi:10.1016/S1352-2310(98)00352-5, 1999.

Neuman, J. A., Huey, L. G., Ryerson, T. B., and Fahey, D. W.: Study of inlet materials for sampling atmospheric nitric acid, Environ. Sci. Technol., 33, 1133–1136, doi:10.1021/es980767f, 1999.

Norman, M., Spirig, C., Wolff, V., Trebs, I., Flechard, C., Wisthaler, A., Schnitzhofer, R., Hansel, A., and Neftel, A.: Intercomparison of ammonia measurement techniques at an intensively managed grassland site (Oensingen, Switzerland), Atmos. Chem. Phys., 9, 2635–2645, doi:10.5194/acp-9-2635-2009, 2009.

Ottley, C. J. and Harrison, R. M.: The spatial distribution and particle size of some inorganic nitrogen, sulphur and chlorine species over the North Sea, Atmos. Environ., 26, 1689–1699, doi:10.1016/0960-1686(92)90067-U, 1992.

Pang, Y., Eatough, N. L., Wilson, J., and Eatough, D. J.: Effect of Semivolatile Material on $PM_{2.5}$ Measurement by the $PM_{2.5}$ Federal Reference Method Sampler at Bakersfield, California, Aerosol Sci. Technol., 36, 289–299, doi:10.1080/027868202753504489, 2002.

Parmar, R., Satsangi, G., Lakhani, A., Srivastava, S., and Prakash, S.: Simultaneous measurements of ammonia and nitric acid in ambient air at Agra (27°10′N and 78°05′E) (India), Atmos. Environ., 35, 5979–5988, doi:10.1016/S1352-2310(00)00394-0, 2001.

Pay, M. T., Jiménez-Guerrero, P., and Baldasano, J. M.: Assessing sensitivity regimes of secondary inorganic aerosol formation in Europe with the CALIOPE-EU modeling system, Atmos. Environ., 51, 146–164, doi:10.1016/j.atmosenv.2012.01.027, 2012.

Perrino, C., Catrambone, M., Di Menno Di Bucchianico, A., and Allegrini, I.: Gaseous ammonia in the urban area of Rome, Italy and its relationship with traffic emissions, Atmos. Environ., 36, 5385–5394, doi:10.1016/S1352-2310(02)00469-7, 2002.

Petetin, H., Beekmann, M., Sciare, J., Bressi, M., Rosso, A., Sanchez, O., and Ghersi, V.: A novel model evaluation approach focusing on local and advected contributions to urban $PM_{2.5}$ levels – application to Paris, France, Geosci. Model Dev., 7, 1483–1505, doi:10.5194/gmd-7-1483-2014, 2014.

Petetin, H., Beekmann, M., Colomb, A., Denier van der Gon, H. A. C., Dupont, J.-C., Honoré, C., Michoud, V., Morille, Y., Perrussel, O., Schwarzenboeck, A., Sciare, J., Wiedensohler, A., and Zhang, Q. J.: Evaluating BC and $NO_x$ emission inventories for the Paris region from MEGAPOLI aircraft measurements, Atmos. Chem. Phys., 15, 9799–9818, doi:10.5194/acp-15-9799-2015, 2015.

Petit, J.-E., Favez, O., Sciare, J., Crenn, V., Sarda-Estève, R., Bonnaire, N., Mocnik, G., Dupont, J.-C., Haeffelin, M., and Leoz-Garziandia, E.: Two years of near real-time chemical composition of submicron aerosols in the region of Paris using an Aerosol Chemical Speciation Monitor (ACSM) and a multi-wavelength Aethalometer, Atmos. Chem. Phys., 15, 2985–3005, doi:10.5194/acp-15-2985-2015, 2015.

Pierson, W. R., Brachaczek, W. W., Japar, S. M., Cass, G. R., and Solomon, P. A.: Dry deposition and dew chemistry in Claremont, California, during the 1985 nitrogen species methods comparison study, Atmos. Environ., 22, 1657–1663, doi:10.1016/0004-6981(88)90393-9, 1988.

Platt, U., Perner, D., Schröder, J., Kessler, C., and Toenissen, A.: The diurnal variation of $NO_3$, J. Geophys. Res., 86, 11965–11970, 1981.

Pleim, J. E., Bash, J. O., Walker, J. T., and Cooter, E. J.: Development and evaluation of an ammonia bidirectional flux parameterization for air quality models, J. Geophys. Res. Atmos., 118, 3794–3806, doi:10.1002/jgrd.50262, 2013.

Pope, C. A., Ezzati, M., and Dockery, D. W.: Fine-particulate air pollution and life expectancy in the United States., N. Engl. J. Med., 360, 376–86, doi:10.1056/NEJMsa0805646, 2009.

Pouliot, G., Pierce, T., Denier van der Gon, H., Schaap, M., Moran, M., and Nopmongcol, U.: Comparing emission inventories and model-ready emission datasets between Europe and North America for the AQMEII project, Atmos. Environ., 53, 4–14, doi:10.1016/j.atmosenv.2011.12.041, 2012.

Putaud, J.-P., Van Dingenen, R., Alastuey, A., Bauer, H., Birmili, W., Cyrys, J., Flentje, H., Fuzzi, S., Gehrig, R., Hansson, H. C., Harrison, R. M., Herrmann, H., Hitzenberger, R., Hüglin, C., Jones, A. M., Kasper-Giebl, A., Kiss, G., Kousa, A., Kuhlbusch, T. A. J., Löschau, G., Maenhaut, W., Molnar, A., Moreno, T., Pekkanen, J., Perrino, C., Pitz, M., Puxbaum, H., Querol, X., Rodriguez, S., Salma, I., Schwarz, J., Smolik, J., Schneider, J., Spindler, G., ten Brink, H., Tursic, J., Viana, M., Wiedensohler, A., and Raes, F.: A European aerosol phenomenology – 3?: Physical and chemical characteristics of particulate matter from 60 rural, urban, and kerbside sites across Europe, Atmos. Environ., 44, 1308–1320, doi:10.1016/j.atmosenv.2009.12.011, 2010.

Reche, C., Viana, M., Pandolfi, M., Alastuey, A., Moreno, T., Amato, F., Ripoll, A., and Querol, X.: Urban $NH_3$ levels and sources in a Mediterranean environment, Atmos. Environ., 57, 153–164, doi:10.1016/j.atmosenv.2012.04.021, 2012.

Sartelet, K., Debry, E., Fahey, K., Roustan, Y., Tombette, M., and Sportisse, B.: Simulation of aerosols and gas-phase species over Europe with the Polyphemus system: Part I – Model-to-data comparison for 2001, Atmos. Environ., 41, 6116–6131, doi:10.1016/j.atmosenv.2007.04.024, 2007.

Schaap, M., Timmermans, R. M. A., Roemer, M., Boersen, G. A. C., Builtjes, P. J. H., Sauter, F. J., Velders, G. J. M., and Beck, J. P.: The LOTOS EUROS model: description, validation and latest developments, Int. J. Environ. Pollut., 32, 270, doi:10.1504/IJEP.2008.017106, 2008.

Schmidt, H. and Derognat, C.: A comparison of simulated and observed ozone mixing ratios for the summer of 1998 in Western Europe, Atmos. Environ., 35, 6277–6297, 2001.

Sciare, J., d'Argouges, O., Zhang, Q. J., Sarda-Estève, R., Gaimoz, C., Gros, V., Beekmann, M., and Sanchez, O.: Comparison between simulated and observed chemical composition of fine aerosols in Paris (France) during springtime: contribution of regional versus continental emissions, Atmos. Chem. Phys., 10, 11987–12004, doi:10.5194/acp-10-11987-2010, 2010.

Sciare, J., D'Argouges, O., Sarda-Estève, R., Gaimoz, C., Dolgorouky, C., Bonnaire, N., Favez, O., Bonsang, B., and Gros, V.: Large contribution of water-insoluble secondary organic aerosols in the region of Paris (France) during wintertime, J. Geophys. Res., 116, D22203, doi:10.1029/2011JD015756, 2011.

Seinfeld, J. H. and Pandis, S. N.: Atmospheric Chemistry and Physics: From Air Pollution to Climate Change, John Wiley, New York, 2006.

Skjøth, C. A., Geels, C., Berge, H., Gyldenkærne, S., Fagerli, H., Ellermann, T., Frohn, L. M., Christensen, J., Hansen, K. M., Hansen, K., and Hertel, O.: Spatial and temporal variations in ammonia emissions – a freely accessible model code for Europe, Atmos. Chem. Phys., 11, 5221–5236, doi:10.5194/acp-11-5221-2011, 2011.

Solomon, P. A., Salmon, L. G., Fall, T., and Cass, G. R.: Spatial and temporal distribution of atmospheric nitric acid and particulate nitrate concentrations in the Los Angeles area, Environ. Sci. Technol., 26, 1594–1601, doi:10.1021/es00032a016, 1992.

Stern, R.: Entwicklung und Anwendung des chemischen Transportmodells REM/CALGRID, Berichte zum UBA Forschungsvorhaben 298 41 252, Freie Universität Berlin, Institut für Meteorologie, 2003.

Stohl, A., Haimberger, L., Scheele, M. P., and Wernli, H.: An intercomparison of results from three trajectory models, Meteorol. Appl., 8, 127–135, doi:10.1017/S1350482701002018, 2001.

Sutton, M., Dragosits, U., Tang, Y., and Fowler, D.: Ammonia emissions from non-agricultural sources in the UK, Atmos. Environ., 34, 855–869, doi:10.1016/S1352-2310(99)00362-3, 2000.

Takahama, S., Wittig, A. E., Vayenas, D. V., Davidson, C. I., and Pandis, S. N.: Modeling the diurnal variation of nitrate during the Pittsburgh Air Quality Study, J. Geophys. Res., 109, D16S06, doi:10.1029/2003JD004149, 2004.

Trebs, I., Meixner, F. X., Slanina, J., Otjes, R., Jongejan, P., and Andreae, M. O.: Real-time measurements of ammonia, acidic trace gases and water-soluble inorganic aerosol species at a rural site in the Amazon Basin, Atmos. Chem. Phys., 4, 967–987, doi:10.5194/acp-4-967-2004, 2004.

Trebs, I., Andreae, M. O., Elbert, W., Mayol-Bracero, O. L., Soto-García, L. L., Rudich, Y., Falkovich, A. H., Maenhaut, W., Artaxo, P., Otjes, R., and Slanina, J.: Aerosol inorganic composition at a tropical site: discrepancies between filter-based sampling and a semi-continuous method, Aerosol Sci. Tech., 42, 255–269, doi:10.1080/02786820801992899, 2008.

Vayenas, D. V., Takahama, S., Davidson, C. I., and Pandis, S. N.: Simulation of the thermodynamics and removal processes in the sulfate-ammonia-nitric acid system during winter: Implications for $PM_{2.5}$ control strategies, J. Geophys. Res., 110, D07S14, doi:10.1029/2004JD005038, 2005.

Vrekoussis, M., Kanakidou, M., Mihalopoulos, N., Crutzen, P. J., Lelieveld, J., Perner, D., Berresheim, H., and Baboukas, E.: Role of the $NO_3$ radicals in oxidation processes in the eastern Mediterranean troposphere during the MINOS campaign, Atmos. Chem. Phys., 4, 169–182, doi:10.5194/acp-4-169-2004, 2004.

Wesely, M. L.: Parameterization of surface resistances to gaseous dry deposition in regional-scale numerical models, Atmos. Environ., 23, 1293–1304, doi:10.1016/0004-6981(89)90153-4, 1989.

Wichink Kruit, R. J., van Pul, W. A. J., Otjes, R. P., Hofschreuder, P., Jacobs, A. F. G., and Holtslag, A. A. M.: Ammonia fluxes and derived canopy compensation points over non-fertilized agricultural grassland in The Netherlands using the new gradient ammonia–high accuracy–monitor (GRAHAM), Atmos. Environ., 41, 1275–1287, doi:10.1016/j.atmosenv.2006.09.039, 2007.

Yao, X., Hu, Q., Zhang, L., Evans, G. J., Godri, K. J., and Ng, A. C.: Is vehicular emission a significant contributor to ammonia in the urban atmosphere?, Atmos. Environ., 80, 499–506, doi:10.1016/j.atmosenv.2013.08.028, 2013.

Yin, J. and Harrison, R. M.: Pragmatic mass closure study for $PM_{1.0}$, $PM_{2.5}$ and $PM_{10}$ at roadside, urban background and rural sites, Atmos. Environ., 42, 980–988, doi:10.1016/j.atmosenv.2007.10.005, 2008.

Zechmeister-Boltenstern, S.: Training on NH3 measurement by wet chemistry techniques, ACTRIS TNA Activity Report, 2010.

Zhang, L., Wright, L. P., and Asman, W. A. H.: Bi-directional air-surface exchange of atmospheric ammonia: A review of measurements and a development of a big-leaf model for applications in regional-scale air-quality models, J. Geophys. Res., 115, D20310, doi:10.1029/2009JD013589, 2010.